



## ORIGINAL ARTICLE

# Characterizing microglial senescence: Tau as a key player

Deniz Karabag<sup>1,2,3</sup> | Hannah Scheiblich<sup>1,2</sup> | Angelika Griep<sup>1,2</sup> | Francesco Santarelli<sup>2</sup> |  
 Stephanie Schwartz<sup>1</sup> | Michael T. Heneka<sup>1,2,4,5</sup>  | Christina Ising<sup>3</sup> 

<sup>1</sup>Department for Neuroimmunology, Institute of Innate Immunity, Medical Faculty, University of Bonn, Bonn, Germany

<sup>2</sup>German Center for Neurodegenerative Diseases (DZNE), Bonn, Germany

<sup>3</sup>Faculty of Medicine and University Hospital Cologne, Cluster of Excellence Cellular Stress Response in Aging-associated Diseases (CECAD), University of Cologne, Cologne, Germany

<sup>4</sup>Luxembourg Centre for Systems Biomedicine (LCSB), University of Luxembourg, Belvaux, Luxembourg

<sup>5</sup>Division of Infectious Diseases and Immunology, University of Massachusetts Medical School, Worcester, Massachusetts, USA

## Correspondence

Michael T. Heneka, Department for Neuroimmunology, Institute of Innate Immunity, Medical Faculty, University of Bonn, Bonn, Germany.

Email: [michael.heneka@uni.lu](mailto:michael.heneka@uni.lu)

Christina Ising, University of Cologne, Faculty of Medicine and University Hospital Cologne, Cluster of Excellence Cellular Stress Response in Aging-associated Diseases (CECAD), Cologne, Germany.

Email: [christina.ising@uk-koeln.de](mailto:christina.ising@uk-koeln.de)

## Funding information

Cluster of Excellence CECAD - Excellent in aging research, Grant/Award Number: EXC 2030 - 390661388; Cluster of Excellence Immunosensation2 - the immune sensory system, Grant/Award Number: EXC 2151 - 390873048

## Abstract

The highest risk factor for the development of neurodegenerative diseases like tauopathies is aging. Many physiological decrements underlying aging are linked to cellular senescence. Senescent cells are characterized by an irreversible growth arrest and formation of a senescence-associated secretory phenotype (SASP), a proinflammatory secretome that modifies the cellular microenvironment and contributes to tissue deterioration. Microglia, the innate immune cells in the brain, can enter a senescent state during aging. In addition, senescent microglia have been identified in the brains of tau-transgenic mice and patients suffering from tauopathies. While the contribution of senescent microglia to the development of tauopathies and other neurodegenerative diseases is a growing area of research, the effect of tau on microglial senescence remains elusive. Here, we exposed primary microglia to 5 and 15 nanomolar (nM) of monomeric tau for 18 h, followed by a recovery period of 48 h. Using multiple senescence markers, we found that exposure to 15 nM, but not 5 nM of tau increased levels of cell cycle arrest and a DNA damage marker, induced loss of the nuclear envelope protein lamin B1 and the histone marker H3K9me3, impaired tau clearance and migration, altered the cell morphology and resulted in formation of a SASP. Taken together, we show that exposure to tau can lead to microglial senescence. As senescent cells were shown to negatively impact tau pathologies, this suggests the presence of a vicious circle, which should be further investigated in the future.

**Abbreviations:** AD, Alzheimer's disease; ALS, Amyotrophic lateral sclerosis; CD11b, cluster of differentiation molecule; CM, conditioned medium; CNS, central nervous system; CXCL-1, chemokine (C-X-C motif) ligand 1; DAPI, 4',6'-diamidino-2-phenylindole; DDR, DNA damage response; DMEM, Dulbecco's modified eagle's medium; ECM, extracellular matrix; FCS, Fetal calf serum; FTD, Frontotemporal dementia; H3K9me2, lysine 9 dimethylation on histone 3; H3K9me3, lysine 9 trimethylation on histone 3; HGPS, Hutchinson-Gilford progeria syndrome; HMCs, human glomerular mesangial cells; IBA1, ionized calcium-binding adapter molecule 1; ILs, Interleukins; JAK, Janus kinase; Lamin B1, nuclear lamina type B1; LSM, Laser scanning microscope; MMPs, matrix metalloproteinases; PBS, Phosphate-buffered saline; PD, Parkinson's disease; PFA, paraformaldehyde; RIPA, Radioimmunoprecipitation assay lysis buffer; RRID, Research Resource Identifier (see [scicrunch.org](https://scicrunch.org)); SASP, senescence-associated secretory phenotype; STAT, signal transducers and activators of transcription; TNF- $\alpha$ , tumor necrosis factor- $\alpha$ ;  $\gamma$ H2AX, phosphorylated histone H2AX.

Michael T. Heneka and Christina Ising have contributed equally to this work.

This is an open access article under the terms of the [Creative Commons Attribution-NonCommercial-NoDerivs](https://creativecommons.org/licenses/by-nc-nd/4.0/) License, which permits use and distribution in any medium, provided the original work is properly cited, the use is non-commercial and no modifications or adaptations are made.

© 2023 The Authors. *Journal of Neurochemistry* published by John Wiley & Sons Ltd on behalf of International Society for Neurochemistry.



## KEYWORDS

aging, cellular senescence, DNA damage, microglia, SASP, tau

## 1 | INTRODUCTION

Worldwide, more than 50-million people suffer from dementia, and in 20 years, approximately 140 million people will be affected. Secondary and primary tauopathies such as Alzheimer's Disease (AD) and Frontotemporal Dementia (FTD), respectively, represent a group of neurodegenerative disorders clinically characterized by dementia and pathologically defined by abnormal accumulation and deposition of tau protein aggregation. Clinically, patients suffering from tauopathy may present with cognitive dysfunction, behavioral deficits, and disturbance of movement and language (Lee et al., 2001; Zhang et al., 2022).

Aging represents the greatest risk factor for most tauopathies and other neurodegenerative disorders. During aging, accumulation of DNA damage and metabolic stress can trigger a process called cellular senescence (Muñoz-Espín & Serrano, 2014). Cellular senescence was introduced by Hayflick and Moorhead in 1961 and can be described as a phenomenon in which a population of cells enters a permanent, irreversible state of proliferation arrest through activation of the major tumor-suppressor pathways p53/p21<sup>WAF1</sup> and p16<sup>INK4a</sup>/Rb (Hayflick & Moorhead, 1961; Muñoz-Espín & Serrano, 2014).

Recent findings demonstrate that senescence is not restricted to proliferation arrest but involves a more dynamic process that evolves over time. As a consequence, a concept describing the transition from quiescence into senescence has been proposed (Fujimaki & Yao, 2020). Quiescence is defined as an reversible, temporary state of proliferation arrest. Quiescence has been proven to be beneficial in a variety of healing processes, whereas senescence has been mainly associated with pathological conditions, such as tissue degeneration during age-related diseases (Di Micco et al., 2021; Velarde & Menon, 2016). Quiescent cells may recover from short-term stress but can passage to senescence upon chronic stress (Alessio et al., 2021). This is in line with observations that prolonged exposure to various intrinsic and extrinsic stressors cause long-term cellular senescence through a continuous DNA damage response (DDR) signaling feedback loop (Garwood et al., 2014; Giunta et al., 2008; Rodier et al., 2009).

The senescent phenotype is not limited to proliferation arrest. Senescent cells present with a potential disease-modifying and specific senescence-associated secretory profile (SASP) upon entering a senescent state (Kiecolt-Glaser et al., 2003; Terzi et al., 2016; Ungerleider et al., 2021). The SASP is characterized by the secretion of various soluble signaling factors (e.g., interleukins (ILs), other cytokines, chemokines, and growth factors), proteases (e.g., matrix metalloproteinases (MMPs)), lipids, insoluble proteins and extracellular matrix (ECM) components (Coppé et al., 2010). A variety of

these factors, including IL-1 $\beta$ , IL-6, and TNF- $\alpha$ , can be detected in the brains of tauopathy mouse models and were associated with the SASP (Bussian et al., 2018; Musi et al., 2018). Additionally, senescent cells present with irregular changes in the nuclear envelope and chromosome distribution. Downregulation of nuclear lamina type B1 (lamin B1), a protein involved in nuclear stabilization and chromatin organization, is a well-accepted senescence-associated biomarker (Freund et al., 2012; Saito et al., 2019). A decline in lamin B1 levels has been reported in murine and human cells undergoing senescence and interestingly, lamin B1 levels were shown to be unaffected during quiescence. Hence, lamin B1 is recognized as a crucial contributor to the transition into senescence (Freund et al., 2012). Phosphorylation of H2AX ( $\gamma$ H2AX) is another widely used senescence marker. The occurrence of  $\gamma$ H2AX is an early response to DNA double-strand breaks that promote a constant DDR, thereby accelerating the aging process through induction of a permanent cell cycle arrest and senescence (Mah et al., 2010).

Neither a well-defined marker nor a consensus on the definition of what constitutes quiescence and senescence has been identified. As a result, the mechanism by which quiescence transits to senescence remains poorly understood. To distinguish quiescence from senescence, the evaluation of multiple markers characterizing the senescent phenotype is crucial.

Microglia—the resident macrophages of the central nervous system (CNS)—are prone to develop a dystrophic (potentially senescent) state during aging and in response to neuropathological conditions (Streit, 2006). Microglia priming as a result of microenvironmental changes during neurodegeneration results in an exaggerated inflammatory response (Heneka et al., 2013; Heneka, Carson, et al., 2015; Heneka, Golenbock, & Latz, 2015), thereby stimulating the aggregation of neurotoxic proteins (Perry & Holmes, 2014). More specifically, it was recently demonstrated that the NLRP3 inflammasome present in microglia contributes to tau aggregation and tau-mediated neurodegeneration through the release of IL-1 $\beta$  (Ising et al., 2019). Additionally, neurons with tau-positive inclusions in the brains of AD patients were shown to be surrounded by dystrophic microglia (Streit et al., 2009). In line with this, a recent study revealed that microglia phagocytosing tau aggregate-containing neurons present with a senescent phenotype afterward (Brelstaff et al., 2021).

It remains unclear, however, whether microglial senescence can evolve as a response to tau. Tau can be present in the extracellular space (Yamada et al., 2011) and to investigate if tau contributes to microglia senescence, we used an in vitro approach in which we examined senescence markers in tau-treated microglia. Here, we demonstrated for the first time that primary mouse microglia display several features of senescence after exposure to tau monomers. Microglia treated with different concentrations of



tau monomers show elevated levels of p21<sup>WAF1</sup> and p16<sup>INK4a</sup>, two widely used markers for the induction of cell cycle arrest in senescent cells (González-Gualda et al., 2021). However, additional markers such as loss of the nuclear envelope protein lamin B1 (Freund et al., 2012; Saito et al., 2019) and heterochromatin H3K9me3 (Sidler et al., 2017; Tsurumi & Li, 2012; Zhang et al., 2021), phosphorylation of histone H2AX (Hernandez-Segura et al., 2018) and formation of a SASP (Coppé et al., 2010) only occurred when treated with higher tau concentrations. In addition, functional assays demonstrated that treatment with higher tau concentrations impaired tau clearance (Brelstaff et al., 2021) and decreased migration time and speed (Caldeira et al., 2014, 2017; Damani et al., 2011). Lastly, exposure to higher tau concentrations resulted in cytoskeleton changes in microglia (Moujabber et al., 2019; Nishio & Inoue, 2005; Reed et al., 2001; Wang, 1985). These findings specify that assessing the classical cell cycle arrest markers alone is not sufficient to study microglia senescence and a more robust characterization, as presented in this study, is required.

## 2 | METHODS

### 2.1 | Study design

No randomization was performed to allocate individual cultures to specific experiments within the study. No sample calculations were performed. This study was exploratory and the sample size was estimated based on similar studies previously carried out in the laboratory for morphology and migration (Scheiblich et al., 2021) as well as studies published by other groups for phagocytosis/clearance (Brelstaff et al., 2021) and the detection of senescence markers (Shang et al., 2020; Yang et al., 2017). Researchers performing the final analysis of immunoblots, immunostainings, tau clearance, migration, and morphology assays were blinded to the treatment groups. No exclusion criteria were predetermined. Samples/data points were excluded from the analysis only if they were identified as outliers using a ROUT test ( $Q=1\%$ ). The  $n$  number ( $n=$ ) specifies the amount of independent primary microglia cell culture preparations.

### 2.2 | Animals

Wildtype C57BL/6N mice (Charles River Laboratories) were housed under standardized conditions in the University Hospital of Bonn animal facility at 22°C and a 12h light-dark cycle with access to food and water ad libitum. Animal care and handling was performed according to the guidelines of animal welfare as laid down by the German Research Council (DFG) and the Declaration of Helsinki. Institutional ethical approval was not required to conduct this study. Pups at postnatal day 0–3 (P0–P3) were decapitated in the morning and the brains harvested. Mixed genders were used and all brains from one litter (average of 6–8 pups per preparation) pooled for the generation of mixed glia cultures, allowing us to shake off microglia

up to three times for different experiments (for details, see "Primary Microglia Culture"). For each biological repeat, an independent litter was used to generate a mixed glia culture. Overall, this approach resulted in the use of 9 litters to conduct this study.

### 2.3 | Primary microglia culture

Primary wildtype mouse microglia cell cultures were prepared as previously described (Venegas et al., 2017). In brief, mixed glial cultures were prepared from the brains of P0–P3 pups. After removing the meninges, brains were washed with HBSS (Gibco™, Cat #24020091) several times before they were incubated with trypsin (LIFE Technologies, Cat #15400054) and DNase I (Roche, Cat #11284932001) for 10 min at 37°C. A single-cell suspension was generated by mechanical shearing before the cells were pelleted and resuspended in an appropriate amount of medium. The cells were cultivated for 7–10 days in DMEM (Gibco™, Cat #31966047) with 10% Fetal Calf Serum (FCS, Gibco™, Cat #26140079), 10% L929 conditioned medium (Merck, Cat #85011425), and 5 U/mL penicillin-streptomycin (Gibco™, Cat #15070063) with 2 brains per poly-L-lysine-coated (PLL, Merck, Cat #P1524) T75 flask. Seven to ten days after cultivation, microglia were shaken at RT by tapping against the flasks multiple times by hand and confirming floating of the cells under the microscope, followed by counting and plating in DMEM (Gibco™, Cat #31966047) supplemented with 1x N2-Supplement (Gibco™, Cat #17502048) and 5 U/mL penicillin-streptomycin (Gibco™, Cat #15070063) overnight before treatment. Microglia were shaken off up to three times.

### 2.4 | Primary microglia treatment

Primary mouse microglia were plated overnight in 6-well plates ( $1.3 \times 10^6$  cells/well) for immunoblotting and collection of conditioned medium, in 12-well plates ( $5 \times 10^5$  cells/well) for RNA isolation, in 24-well plates for clearance ( $3.5 \times 10^5$  cells/well) or migration assays ( $5 \times 10^5$  cells/well) and on 13 mm<sup>2</sup> coverslips in 24-well plates ( $1\text{--}1.5 \times 10^5$  cells/well) for immunocytochemistry and morphology analysis. The following day, cells were gently washed with Dulbecco's phosphate-buffered saline (DPBS; Gibco™, Cat #14190169) and treated with 5 or 15 nM of recombinant human wildtype (2N4R) tau for 18 h, washed and cultured for another 48 h. As the tau preparations were directly dissolved in medium, the control treatment was performed using only medium. Additionally, cells were treated with 50 ng/mL of phorbol 12-myristate 13-acetate (PMA; Sigma-Aldrich, Cat #16561-29-8) (diluted from stock in medium) for 72 h. All treatments were done in DMEM (Gibco™, Cat #31966047) supplemented with 1x N2-Supplement (Gibco™, Cat #17502048) and 5 U/mL penicillin-streptomycin (Gibco™, Cat #15070063) and performed simultaneously on cells in individual wells. For each experiment, 3–4 biologically independent experiments were performed using

independently prepared mixed glia cultures for shaking off microglia. In each independent experiment, individual wells were assessed. Samples were not pooled.

## 2.5 | Immunoblotting

At the end of the experimental procedure, the microglia were washed with ice-cold 1x PBS and lysed in appropriate volumes of 1x Radio-Immunoprecipitation Assay Lysis Buffer (RIPA) buffer (50mM Tris-HCl, 1% Triton X-100, 0.5% sodium deoxycholate, 0.1% sodium dodecyl sulfate (SDS) with protease/phosphatase inhibitor (Thermo Scientific™, Cat #78441)). Samples were transferred to a tube on ice for 30min and vortexed a few times in between. Afterward, samples were centrifuged at 20000  $\times g$  for 15 min at 4°C. Protein quantification was performed using a BCA Protein Assay Kit (Thermo Scientific™, Cat #23225) on the supernatants containing the soluble proteins. For immunoblot analysis, samples were supplemented with 1x NuPAGE sample buffer (Thermo Scientific™, Cat #R1381), heated for 5 min at 95°C and loaded on 4%–12% NuPAGE Novex gels (Invitrogen™, Cat #NP0323BOX) containing 25  $\mu g$  protein per sample. After transfer of proteins to nitrocellulose blotting membranes (Thermo Scientific™, Cat #PB7220), membranes were blocked in 3% Bovine Serum Albumin (BSA) (Rockland, Fraction V, Cat #BSA-1000) in Tris-buffered saline supplemented with Tween-20 (TBST; 10mM Tris-HCl, 150mM NaCl, 0.05% Tween-20, pH8.0) for 1h, followed by incubation with primary antibodies anti-p21 (Abcam, Cat #ab218311, [RRID:AB\\_2890611](#)) (1:1000), anti-p16 (Abcam, Cat #ab211542, [RRID:AB\\_2891084](#)) (1:1000) and anti-lamin B1 (Proteintech, Cat #66095-1-Ig, [RRID:AB\\_11232208](#)) (1:1000) in blocking solution overnight at 4°C. Incubation with anti-GAPDH (Sigma-Aldrich Cat #G9545, [RRID:AB\\_796208](#)) (1:5000) was done in blocking solution for 1h at RT. Proteins were visualized by fluorescent-tagged secondary antibodies (LI-COR). Imaging was performed by using a LI-COR ODYSSEY CLx. Data were analyzed with ImageStudio software version 5.2.5 (LI-COR). Individual experiments were run on separate blots. The protein amounts on every blot were normalized to GAPDH first and then normalized to the averaged value obtained for control microglia before all data were combined. PageRuler™ Prestained Protein Ladder (Thermo Scientific™, Cat #26616) was used as a molecular weight marker.

## 2.6 | Preparation of recombinant human tau

Recombinant human wildtype tau (2N4R) was cloned into pRK172 and the purification was performed as described previously (Ising et al., 2019). In brief, the tau-expressing inducible plasmids were transformed into BL21(DE3) *E. coli* (Agilent, Cat #230245). Tau expression was induced by adding IPTG (Merck, Cat# I6758) to a liquid culture of a single colony. Bacteria containing tau were pelleted (3810  $\times g$  for 10min at 4°C) followed by resuspension of the pellet in BRB-80 (80mM PIPES, 1mM magnesium sulfate, 1mM

EGTA, pH6.8) supplemented with 0.1% 2-mercapthoethanol and 1mM PMSF. After sonication (4cycles of 1 min with 2 min on ice in between), bacterial debris were removed by centrifugation (20min, 3810  $\times g$  at 4°C). The tau-containing supernatant was boiled for 10min and centrifuged again. The tau protein was further purified by cation exchange chromatography using sepharose fast-flow beads (Merck, Cat #GE17-0729-01). Afterwards, tau was eluted using different concentrations of sodium chloride dissolved in BRB-80 supplemented with 0.1% 2-mercaptoethanol. After testing the presence of tau using a Coomassie gel stain, tau-containing fractions were combined and concentrated in 10mM ammonium bicarbonate buffer using Amicon ultra centrifugal units (10-kDa molecular weight cut-off, Merck, Cat #UFC9010). The resulting tau preparation was tested for the presence of endotoxins using an endotoxin quantification kit (Thermo Fisher Scientific, Cat #A39552S). Tau protein concentration was assessed by a BCA assay (Thermo Fisher Scientific, Cat #23225) before aliquoting. Tau samples were dried in a speed vac before storage at –80°C. Tau proteins were resuspended in DMEM supplemented with 1x N2-Supplement and 5U/mL penicillin–streptomycin right before use.

## 2.7 | Fluorescent labeling of recombinant human tau

Purified recombinant tau was reconstituted in DPBS (Gibco™, Cat #14190169) to a final concentration of 8  $\mu M$ . After addition of 0.025mg Alexa Fluor™ 405 NHS ester (Thermo Fisher Scientific, Cat #A30000), the solution was incubated for 1h at RT and then placed on an overhead shaker overnight at 4°C. Glycine was added to a final concentration of 100mM, followed by incubation for 1h at RT. The solution was dialyzed in 1x PBS (2x 2h at RT) using a 10K MWCO dialysis cassette (Thermo Fisher Scientific, Cat #66383). Labeled tau was aliquoted in protein low-binding tubes (Eppendorf™, Cat #0030108116) and stored at –80°C for single use.

## 2.8 | Assessment of the SASP

Conditioned medium (CM) was collected from the cells that were subsequently used for protein analysis and centrifuged at 300  $\times g$  for 5min at 4°C to remove cellular debris. The concentration of proinflammatory factors in the CM was determined using the Mouse IL-1 beta/IL-1F2 DuoSet ELISA (R&D Systems, Cat #DY401), Mouse IL-6 DuoSet ELISA (R&D Systems, Cat #DY406), V-PLEX Plus Proinflammatory Panel 1 Kit (Meso Scale Diagnostics, Cat#K15048G-1) and V-PLEX Cytokine Panel 1 Mouse Kit (Meso Scale Diagnostics, Cat #K15245D-1) according to the manufacturer's recommendations. CM of at least three biologically independent experiments (i.e., at least three independent cell culture preparations) were run on the same plate with two technical replicates per sample, which were averaged before statistical analysis.





## 2.9 | Immunocytochemistry

Cells were fixed in 4% paraformaldehyde (PFA, Merck, Cat #P6148) dissolved in PBS and permeabilized with PBS containing 0.1% Triton X-100 (PBS-T) for 10min each. Blocking was performed using PBS-T containing 3% bovine serum albumin (BSA, Rockland, Fraction V, Cat #BSA-1000) and 5% goat serum (Abcam, Cat #ab7481) for 30min. The primary antibodies rabbit anti-IBA1 (FUJIFILM Wako Shibayagi, Cat #019-19741, [RRID:AB\\_839504](#)) (1:1000), rat anti-CD11b (Bio-Rad, Cat #MCA711, [RRID:AB\\_321292](#)) (1:250), mouse anti-yH2AX (Millipore, Cat #05-636, [RRID:AB\\_309864](#)) (1:100) and rabbit anti-H3K9me3 (Abcam, Cat #ab8898, [RRID:AB\\_306848](#)) (1:200) were applied in blocking solution overnight at 4°C. The secondary antibodies goat anti-rabbit-AlexaFluor594 (Invitrogen™, Cat #A-11012, [RRID:AB\\_2534079](#)) (1:500), goat anti-mouse-AlexaFluor488 (Invitrogen™, Cat #A-11001, [RRID:AB\\_2534069](#)) (1:500) and goat anti-rat-AlexaFluor594 (Invitrogen™, Cat #A-11007, [RRID:AB\\_10561522](#)) (1:500) were applied for 1h at RT. Washing steps in between were done 3 times for 5min in PBS. ProLongGold with 4',6-diamidino-2-phenylindole (DAPI) (Invitrogen™, Cat #P36931) was used as a mounting medium. Z-stack images were taken using a 40x objective on a Zeiss Laser Scanning Microscope 900 (LSM900). Acquired images were processed using ImageJ/Fiji software version 2.0. A manual threshold was set and applied to all images. The nucleus was set as a region of interest (ROI). Intensity of yH2AX and H3K9me3 inside the nucleus (ROI) was calculated by area \* IntDen. Three to four images were captured in the mid-center of the coverslip, which contained optimal cell density. No other inclusion or exclusion criteria were applied.

## 2.10 | Real-time RT-PCR

To isolate RNA, the CM was discarded and cells were washed with 1x PBS before QIAzol Lysis Reagent (Qiagen, Cat# 79306) was added to primary cultured microglia. The homogenate was incubated for 5min at RT, followed by addition of chloroform. Samples were shaken vigorously and centrifuged for 15min at 12000 xg at 4°C. The aqueous phase was collected for RNA isolation using a miRNeasy Micro Kit (Qiagen, Cat #217084) according to the manufacturer's instructions. RNA concentration and purity were quantified spectrophotometrically. Four hundred nanograms of total RNA was reverse transcribed using the High-Capacity cDNA Reverse Transcription Kit (Applied Biosystems, Cat #4368814). The cDNA was amplified in TaqMan gene expression master mix (Applied Biosystems, Cat #4369016) with predeveloped TaqMan assays and reagents according to the manufacturer's instructions. Reactions were carried out using primer sets for *Cdkn1a* (Applied Biosystems™, Mm00432448\_m1), *Cdkn2a* (Applied Biosystems™, Mm00494449\_m1), *Lmn1* (Applied Biosystems™, Mm00521949\_m1) and 18S rRNA (Applied Biosystems™, Cat #4310893E), which was used as a loading control for all reactions. Subsequent analyses were performed using the RT-PCR System StepOnePlus™ together with the StepOne™ software (both from Applied Biosystems™). Transcript levels were quantified

by the comparative  $\Delta\Delta C_T$  method. All gene expression data shown in a respective graph were generated from cDNA originating from independent cell culture preparations, but run together on one RT-PCR plate with two technical repeats of each sample. The average of the technical repeats was used for statistical analysis.

## 2.11 | Tau clearance assay

After tau exposure and recovery, microglia were treated with 0.2  $\mu$ M AlexaFluor-405-labeled tau monomers and incubated for 30–60min. Uptake was stopped by one washing step with 1x PBS to remove free tau and cells were harvested using 0.5% trypsin (Thermo Fisher Scientific, Cat #15400054). Blocking solution containing PBS and FCS (Gibco™, Cat #10500064) (1:1 ratio) was applied for 10min on ice. Cells were then labeled with the allophycocyanin anti-mouse/human CD11b antibody (BioLegend Cat #101212, [RRID:AB\\_312795](#)) (1:100) for 30min in FACS buffer (1x PBS supplemented with 2% FCS) on ice. After labeling, cells were collected, resuspended in 300  $\mu$ L ice-cold FACS buffer, and measured by flow cytometry using the FACSCanto II and the FACSDiva software (Becton Dickinson, Heidelberg, Germany). Tau clearance was then analyzed and quantified using FlowJo (v3.05470; Ashland, OR). Each biologically independent experiment was performed with three technical repeats, which were averaged before statistical analysis of the data was performed.

## 2.12 | Migration assay

A migration assay was performed by the method of Liang and colleagues (Liang et al., 2007). Briefly, after tau exposure and recovery, the confluent cell monolayer was scraped with a pipet tip to create a scratch, followed by a wash with 1x PBS. Cells were incubated for 8h in 1mL DMEM supplemented with 1x N2. Images were acquired using a Nikon ECLIPSE Ti brightfield microscope at desired times in a marked sector as reference area. Images were taken at 10x magnification and migration was calculated by dividing scratch widths measured before and after incubation, quantified at 20 distinct locations within the reference area. Image analysis was performed using ImageJ/Fiji software version 2.0.

## 2.13 | Morphology

After tau exposure and recovery, the cells were fixed in 4% PFA, washed 3 times in PBS containing PBS-T, and stained with Alexa Fluor™ 647 Phalloidin (Invitrogen™, Cat #A22287, [RRID:AB\\_2620155](#)) (1:100) and DAPI (Thermo Scientific™, Cat #62247) (0.1  $\mu$ g/mL) for 30min in PBS-T. Cells were then mounted and images were taken using a Nikon ECLIPSE Ti fluorescence microscope equipped with a 20x objective. Approximately 20 cells were analyzed per image. A total of five images per condition were taken in



each individual experiment. Cytoskeletal changes were analyzed using CellProfiler (v3.1.8, Broad Institute of Harvard and MIT, MA, USA) (Kamentsky et al., 2011).

## 2.14 | Statistics

At least three independent primary cell culture preparations (*n*) were used for each experiment. Data were evaluated using Graph Pad Prism (version: 9.4.1 (681)) and presented as mean+SD (parametric data) or median+95% CI (nonparametric data) of at least three biologically independent cell culture preparations (*n*). Assessment of the normality (Shapiro–Wilk test) of the data and test for outlier ROUT (*Q*=1%) was performed. Statistical significance for parametric data was analyzed by two-tailed unpaired *t*-test for comparison of two groups, one-way ANOVA with post hoc Tukey's test to compare three groups, or two-way ANOVA with multiple comparisons regardless of rows and columns when data with two variables were analyzed. For nonparametric data, Kruskal–Wallis test with post hoc Dunn's test was applied. Statistical significance was assumed for *p*<0.05. Statistical details for all experiments can be found in the respective figure legends.

## 3 | RESULTS

### 3.1 | Microglia showed a senescent-like phenotype after tau exposure

To clarify the effect of tau on microglial senescence, we exposed primary murine microglia to 5 nM and 15 nM of recombinant human tau monomers and investigated classical senescence markers at both RNA and protein level. While both tau concentrations did not result in increased cytotoxicity (Figure S1), microglia exposed to 15 nM of tau expressed higher *Cdkn2a* RNA levels (Protein name: p16<sup>INK4a</sup>) compared to control and tau 5 nM conditions (Figure 1a). Neither 5 nM nor 15 nM of tau altered gene expression levels of *Cdkn1a* (Figure 1b) (Protein name: p21<sup>WAF1</sup>) or *Lmnbl* (Protein name: lamin B1) (Figure 1c). At the protein level (Figure 1d), however, microglia expressed increased levels of p16<sup>INK4a</sup> and p21<sup>WAF1</sup> independent of the tau concentration (Figure 1e,f). Interestingly, loss of lamin B1 on the protein level only occurred after treatment with tau 15 nM (Figure 1g).

### 3.2 | Characterization of a microglial SASP

Although p16<sup>INK4a</sup> and p21<sup>WAF1</sup> are key pathways involved in cell cycle arrest, it is important to avoid the misconception that cell cycle arrest equals senescence as it can also be a sign of quiescence (Blagosklonny, 2011, 2012; Terzi et al., 2016). In contrast to quiescent cells, senescent cells become hyperfunctional and affect other cells in an autocrine and paracrine fashion through the release of a SASP, thereby contributing to the detrimental effects on tissue loss and degeneration seen in aging and age-related diseases (Coppé

et al., 2010; Cuollo et al., 2020). To investigate the presence of SASP factors in our model system, we measured several previously identified SASP molecules, namely IL-1 $\beta$ , IL-6, TNF- $\alpha$ , IL-15, and CXCL1 (Coppé et al., 2010; Schafer et al., 2020; Su et al., 2021). Interestingly, exposure to 15 nM, but not 5 nM of tau resulted in enhanced secretion of these factors (Figure 2a–e). We confirmed secretion of IL-1 $\beta$ , IL-6, and TNF- $\alpha$  also from senescent microglia using a second model, in which we used phorbol-12-myristat-13-acetat (PMA) to induce senescence (Figure S2), underlining the universal importance of these SASP factors. Additionally, we detected an increase in IL-27 with 15 nM tau, a factor that to the best of our knowledge has not been associated with the SASP so far (Figure 2f). In contrast to showing an increased secretion only upon 15 nM tau treatment, IL-33 secretion was increased dose-dependently while anti-inflammatory IL-10 was decreased in a dose-dependent manner from microglia upon tau treatment (Figure 2g,h).

### 3.3 | Microglia exhibited nuclear changes upon tau treatment

The reduction in protein levels of the nuclear envelope marker lamin B1 prompted us to investigate nuclear changes associated with senescence. Loss of lysine 9 trimethylation on histone H3 (H3K9me3) has previously been associated with tauopathies (Gil et al., 2021; Jury et al., 2020) and cellular senescence (Sidler et al., 2017; Tsurumi & Li, 2012; Zhang et al., 2021). In our model system, we found that exposure to 15 nM, but not 5 nM of tau induced a significant loss of H3K9me3 in microglia (Figure 3a,b). In addition, phosphorylation of histone H2AX (yH2AX), a prominent marker of the DDR and subsequent senescence (Mah et al., 2010), is increased in the brains of AD patients and tau-transgenic mice (Farmer et al., 2020; Musi et al., 2018). Moreover, neurons stimulated with tau oligomers show increased expression of yH2AX (Farmer et al., 2020). Here, we found that exposure to 15 nM, but not 5 nM of tau, resulted in accumulation of nuclear yH2AX foci (Figure 3c,d).

### 3.4 | Senescent microglia presented with reduced capabilities to clear tau

The main functions of microglia are to repair injury, modulate and shape neuronal synapses and maintain CNS homeostasis. Phagocytosis and clearance, which can be compromised in senescent cells (Brelstaff et al., 2021), is an important mechanism used by microglia to exert these functions (Colonna & Butovsky, 2017; Galloway et al., 2019). Therefore, we assessed the ability of microglia to clear tau monomers after tau-mediated senescence induction. First, we induced senescence as previously described, followed by adding fluorescently-labeled tau monomers for 30 or 60 min to the cells before we analyzed them for their tau content using flow cytometry (Figure 4a–f). Here, we demonstrate that treatment with 15 nM, but not 5 nM tau, resulted in a decline in the amount of tau inside of microglia (Figure 4e) and significantly lower numbers of tau-containing cells (Figure 4f) at

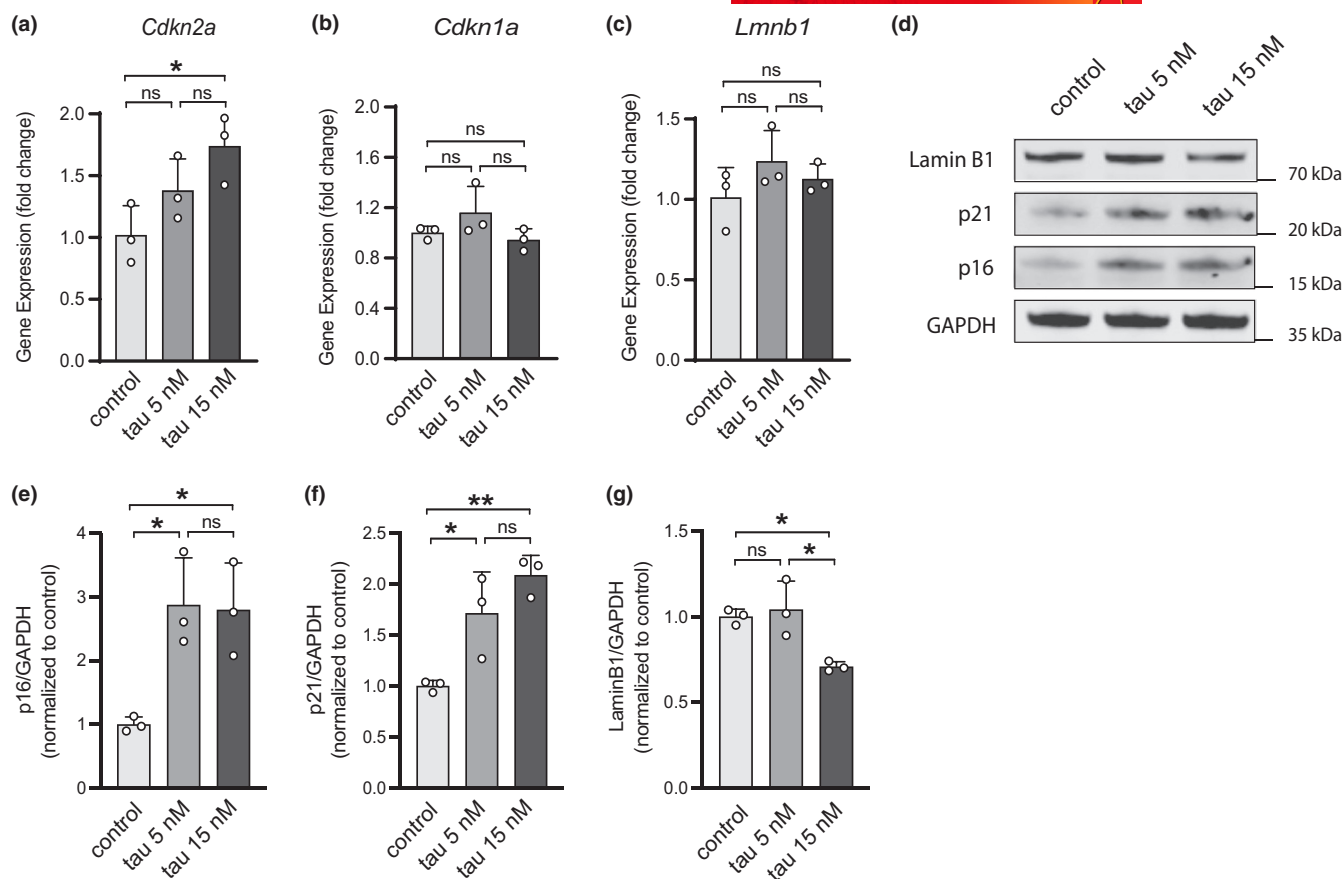


**FIGURE 1** Tau induced markers of cell cycle arrest and loss of lamin B1 in primary mouse microglia. (a–c) Quantification of *Cdkn2a* (p16<sup>INK4a</sup>) (a; control vs. tau 5 nM:  $p=0.2789$ , control vs. tau 15 nM:  $p=0.0333$ , tau 5 nM vs. tau 15 nM:  $p=0.2802$ ), *Cdkn1a* (p21<sup>WAF1</sup>) (b; control vs. tau 5 nM:  $p=0.3652$ , control vs. tau 15 nM:  $p=0.8676$ , tau 5 nM vs. tau 15 nM:  $p=0.1953$ ) and *LmnB1* (c; control vs. tau 5 nM:  $p=0.2847$ , control vs. tau 15 nM:  $p=0.6850$ , tau 5 nM vs. tau 15 nM:  $p=0.6994$ ) RNA levels. (d) Representative immunoblot analysis of lamin B1, p21<sup>WAF1</sup>, p16<sup>INK4a</sup> and GAPDH in tau-treated microglia. (e–g) Quantification of p16<sup>INK4a</sup> (e; control vs. tau 5 nM:  $p=0.0213$ , control vs. tau 15 nM:  $p=0.0255$ , tau 5 nM vs. tau 15 nM:  $p=0.9865$ ), p21<sup>WAF1</sup> (f; control vs. tau 5 nM:  $p=0.0351$ , control vs. tau 15 nM:  $p=0.0053$ , tau 5 nM vs. tau 15 nM:  $p=0.2635$ ) and lamin B1 (g; control vs. tau 5 nM:  $p=0.8649$ , control vs. tau 15 nM:  $p=0.0276$ , tau 5 nM vs. tau 15 nM:  $p=0.0153$ ). Graphs are presented as mean + SD and analyzed by one-way ANOVA (a:  $F(2,6)=5.791$ ,  $p=0.0397$ ; b:  $F(2,6)=2.135$ ,  $p=0.1994$ ; c:  $F(2,6)=1.422$ ,  $p=0.3122$ ; e:  $F(2,6)=9.187$ ,  $p=0.0149$ ; f:  $F(2,6)=13.49$ ,  $p=0.0060$ ; g:  $F(2,6)=9.879$ ,  $p=0.0126$ ) followed by Tukey's test. ns = not significant,  $n=3$  independent cell culture preparations. ROUT test ( $Q=1\%$ ) showed no outliers. No exclusion criteria were predetermined and no samples were excluded from the analysis.

both time points analyzed. Overall, microglia treated with 15 nM tau showed a reduced capability to clear tau.

### 3.5 | Senescent microglia showed an impaired migration rate

Under physiological conditions, microglia show a ramified morphology with highly motile branches to survey the microenvironment (Zhang et al., 2016). However, after a pathogenic event, such as an insult to the central nervous system (CNS), microglia adopt a reactive amoeboid shape, which supports proper migration to the site of injury (Kettenmann et al., 2011; Scheiblich & Bicker, 2015). Interestingly, aging and cellular senescence were associated with impairments in the rate of migration in several cell types including microglia (Caldeira et al., 2014, 2017; Damani et al., 2011). In this

study, we used an in vitro scratch wound assay to measure microglial migration after senescence induction. We found that exposure to 15 nM, but not 5 nM of tau monomers significantly reduced the distance traveled toward the site of insult (Figure 5a,b) as well as the overall speed of microglial migration (Figure 5c).

### 3.6 | Reorganization of the cytoskeleton in senescent microglia

The disturbances in migratory behavior of senescent cells might be the result of reorganizations in the cytoskeleton (Moujaber et al., 2019; Nishio & Inoue, 2005; Reed et al., 2001; Wang, 1985). Senescent cells are characterized by morphological changes, such as enlargements in the cell size (Greenberg et al., 1977; Wallis et al., 2022), but an extensive characterization of the morphology

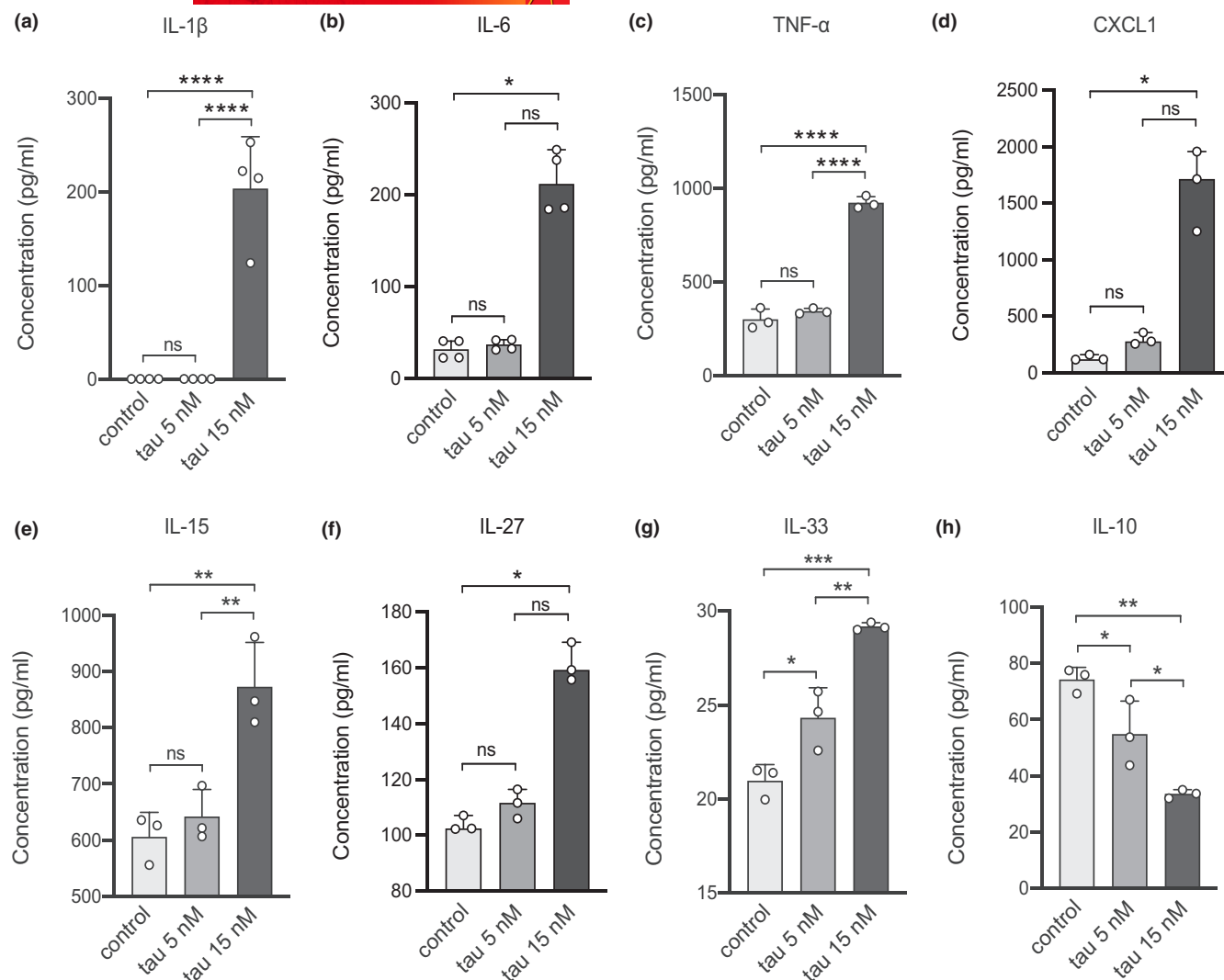


**FIGURE 2** Tau induced a senescence-associated secretory profile (SASP) in primary mouse microglia. (a-h) Exposure to tau monomers induced the release of (a) Interleukin-1 $\beta$  (IL-1 $\beta$ ; control vs. tau 5 nM:  $p > 0.9999$ , control vs. tau 15 nM: \*\*\*\* $p < 0.0001$ , tau 5 nM vs. tau 15 nM: \*\*\*\* $p < 0.0001$ ), (b) Interleukin-6 (IL-6; control vs. tau 5 nM:  $p > 0.9999$ , control vs. tau 15 nM: \* $p = 0.0179$ , tau 5 nM vs. tau 15 nM:  $p = 0.1484$ ), (c) Tumor necrosis factor-alpha (TNF- $\alpha$ ; control vs. tau 5 nM:  $P = 0.4034$ , control vs. tau 15 nM: \*\*\*\* $p < 0.0001$ , tau 5 nM vs. tau 15 nM: \*\*\*\* $p < 0.0001$ ), (d) Chemokine (C-X-C motif) ligand 1 (CXCL1, control vs. tau 5 nM:  $p = 0.5391$ , control vs. tau 15 nM: \* $p = 0.0219$ , tau 5 nM vs. tau 15 nM:  $p = 0.5391$ ), (e) Interleukin-15 (IL-15; control vs. tau 5 nM:  $p = 0.7474$ , control vs. tau 15 nM: \*\* $p = 0.0035$ , tau 5 nM vs. tau 15 nM: \*\* $p = 0.0073$ ), (f) Interleukin-27 (IL-27; control vs. tau 5 nM:  $p = 0.8902$ , control vs. tau 15 nM: \* $p = 0.0338$ , tau 5 nM vs. tau 15 nM:  $p = 0.4081$ ) and (g) Interleukin-33 (IL-33; control vs. tau 5 nM: \* $p = 0.0189$ , control vs. tau 15 nM: \*\*\* $p = 0.0002$ , tau 5 nM vs. tau 15 nM: \*\* $p = 0.0032$ ) and inhibited release of (h) Interleukin-10 (IL-10; control vs. tau 5 nM: \* $p = 0.0396$ , control vs. tau 15 nM: \*\* $p = 0.0012$ , tau 5 nM vs. tau 15 nM: \* $p = 0.0269$ ). Graphs are presented as mean + SD (a, c, e, g, h) or median  $\pm$  95% confidence interval (CI) (b, d, f) and statistical significance for parametric data was analyzed by one-way ANOVA followed by Tukey's test (a:  $F(2,9) = 53.74$ ,  $p < 0.0001$ ; c:  $F(2,6) = 252.4$ ,  $p < 0.0001$ ; e:  $F(2,6) = 18.03$ ,  $p = 0.0029$ ; g:  $F(2,6) = 45.98$ ,  $p = 0.0002$ ; h:  $F(2,6) = 23.44$ ,  $p = 0.0015$ ) and for nonparametric data, Kruskal-Wallis test with post hoc Dunn's test (b: Kruskal-Wallis = 8.028,  $p = 0.0040$ ; d: Kruskal-Wallis = 7.200,  $p = 0.0036$ ; f: Kruskal-Wallis = 6.489,  $p = 0.0107$ ).  $n = 3$  independent cell culture experiments (c-h) or  $n = 4$  independent cell culture experiments (a, b). ns = not significant. ROUT test ( $Q = 1\%$ ) showed no outliers. No exclusion criteria were predetermined and no samples were excluded from the analysis.

of senescent microglia is lacking. Therefore, we stained microglia with the cytoskeleton marker Phalloidin and analyzed cell morphology (Figure 6a,b). Here, we report that exposure to 15 nM, but not 5 nM of tau significantly increased the total skeletal length ( $\mu\text{m}$ ) (Figure 6c), area ( $\mu\text{m}^2$ ) (Figure 6d), perimeter ( $\mu\text{m}$ ) (Figure 6e), number of trunks (No. of Trunks) (Figure 6f) and branches (No. of Branches) (Figure 6g) in primary microglia.

## 4 | DISCUSSION

Cellular senescence is a pleiotropic cell fate that stimulates embryonic development and tissue healing in early life but promotes tissue degeneration and age-related diseases in late life. Senescent cells are characterized by increased DNA damage, impaired DNA damage repair, alterations in kinases involved in cell cycle arrest, and



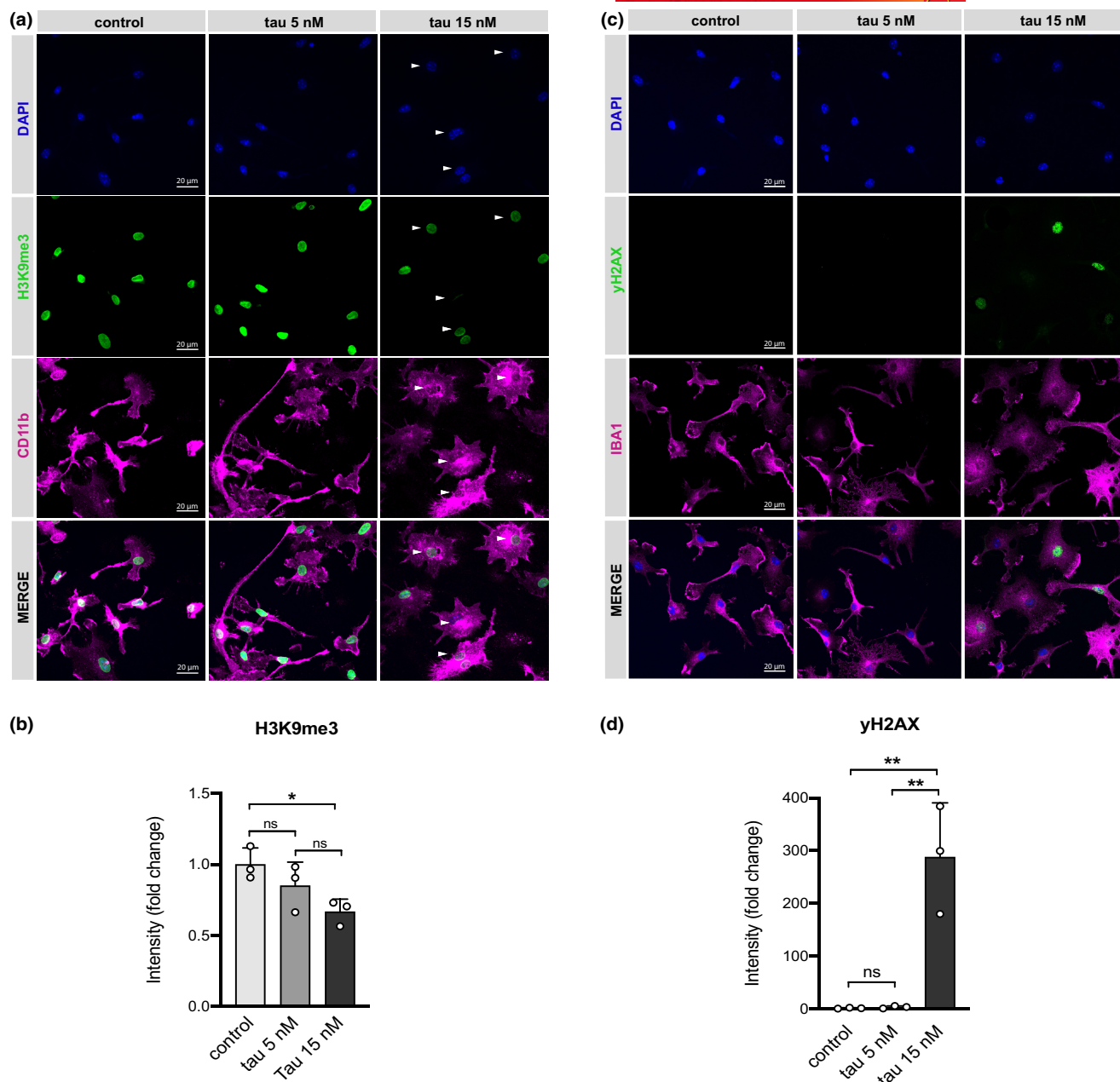


**FIGURE 3** Tau exposure resulted in loss of H3K9me3 and increased phosphorylation of histone H2AX. (a) Representative immunohistochemical staining for trimethylation of lysine 9 on histone 3 (H3K9me3; green), cluster of differentiation molecule (CD11b; magenta) and 4',6-diamidino-2-phenylindole (DAPI; blue) in primary mouse microglia after exposure to different doses of tau. (b) Quantification of H3K9me3 (control vs. tau 5 nM:  $p=0.3797$ , control vs. tau 15 nM:  $p=0.0425$ , tau 5 nM vs. tau 15 nM:  $p=0.2606$ ). (c) Representative immunohistochemical staining for phosphorylated H2AX (yH2AX; green), IBA1 (magenta) and DAPI (blue) in primary mouse microglia after exposure to different concentrations of tau. (d) Quantification of yH2AX (control vs. tau 5 nM:  $p=0.9943$ , control vs. tau 15 nM:  $p=0.0024$ , tau 5 nM vs. tau 15 nM:  $p=0.0026$ ). Graphs are presented as mean + SD and analyzed by one-way ANOVA (b:  $F(2,6)=5.142$ ,  $p=0.0500$ ; d:  $F(2,6)=23.24$ ,  $p=0.0015$ ) with Tukey's test. Arrow heads indicate nuclei with reduced H3K9me3 expression. ns = not significant,  $n=3$  independent cell culture preparations. ROUT test ( $Q=1\%$ ) showed no outliers. No exclusion criteria were predetermined and no samples were excluded from the analysis.

formation of a SASP (Ben-Porath & Weinberg, 2005; Campisi & Di Fagagna, 2007). A few decades ago, increased *Cdkn2a* ( $p16^{\text{INK4a}}$ ) gene expression levels were observed in the brains of AD patients (Arendt et al., 1996; McShea et al., 1997). More recently, elevated levels of  $p16^{\text{INK4a}}$  and yH2AX as well as increased SASP gene

expression levels, including *Il1b*, *Tnfa* and *Cxcl1*, were demonstrated in a tauopathy mouse model (Musi et al., 2018). Additionally, microglia and astrocytes were reported to show increased gene expression levels of *Cdkn2a* ( $p16^{\text{INK4a}}$ ) and *Il6* in another tauopathy mouse model (Bussian et al., 2018).



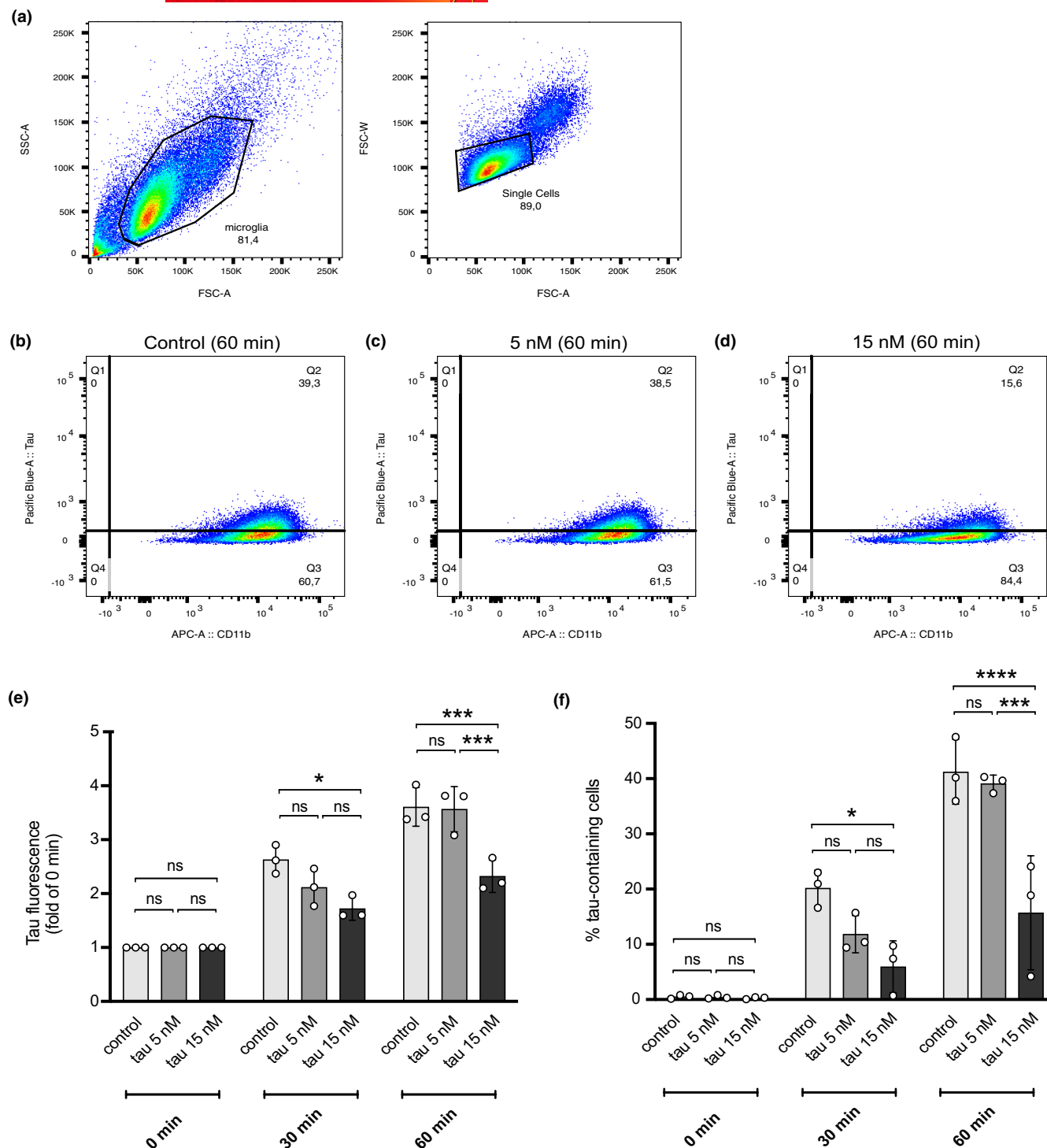


**FIGURE 4** Senescent microglia were impaired in their ability to clear tau monomers. (a) Representative gating scheme for the assessment of tau clearance as measured by flow cytometry. (b–d) Charts representing the engulfment of tau after 60 min by control microglia (b) or microglia pre-exposed to tau monomers (c, d). (e) Quantification of tau fluorescence in the microglia after exposure to 0.2 μM AlexaFluor-405-labeled tau monomers for 0, 30 (control vs. tau 5 nM:  $p=0.3556$ , tau 5 nM vs. tau 15 nM:  $p=0.6661$ , control vs. tau 15 nM:  $*p=0.0124$ ) and 60 minutes (control vs. tau 5 nM:  $p>0.9999$ , tau 5 nM vs. tau 15 nM:  $***p=0.0005$ , control vs. tau 15 nM:  $***p=0.0003$ ). (f) Quantification of the percentage (%) of tau-containing microglia after exposure to tau monomers for 0, 30 (control vs. tau 5 nM:  $p=0.4227$ , tau 5 nM vs. tau 15 nM:  $p=0.8044$ , control vs. tau 15 nM:  $*p=0.0268$ ) and 60 minutes (control vs. tau 5 nM:  $p=0.9996$ , tau 5 nM vs. tau 15 nM:  $***p=0.0002$ , control vs. tau 15 nM:  $****p<0.0001$ ). Graphs are presented as mean+SD and analyzed by two-way ANOVA with multiple comparisons regardless of rows and columns (e:  $F(2,18)=18.51$ ,  $p<0.0001$ ; f:  $F(2,18)=20.60$ ,  $p<0.0001$ ). ns=not significant,  $n=3$  independent cell culture preparations. ROUT test ( $Q=1\%$ ) showed no outliers. No exclusion criteria were predetermined and no samples were excluded from the analysis.

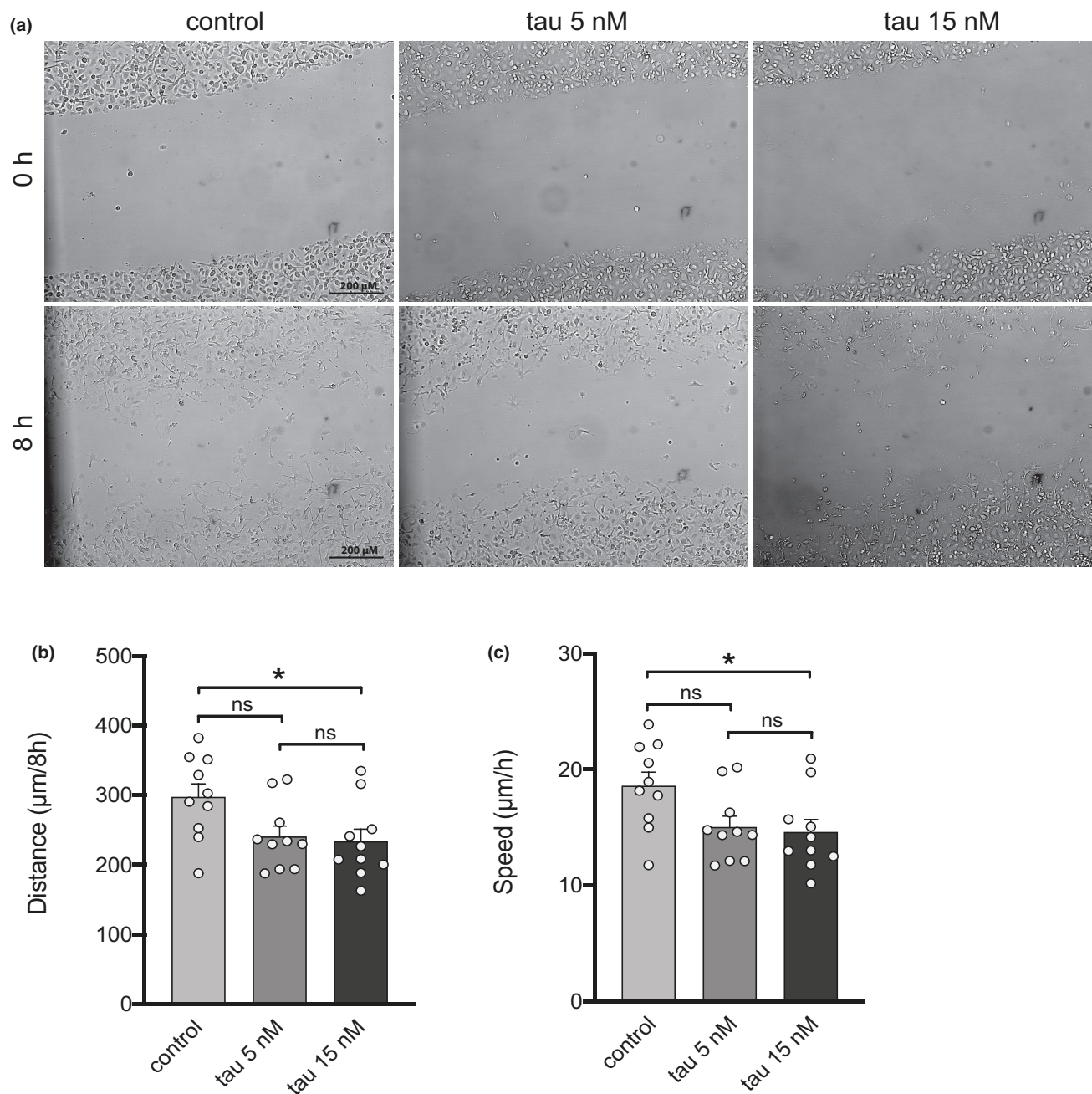


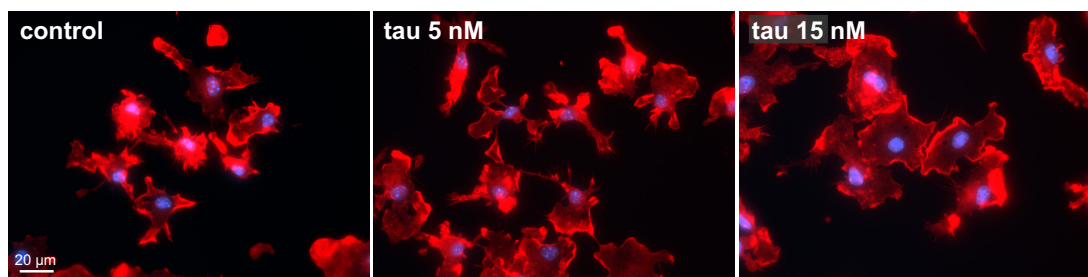
**FIGURE 5** Senescent microglia showed reduced migration distance and speed. (a) Representative time course images of an in vitro microglial scratch assay at 0 and 8 h. (b) Analysis of the total migration distance in  $\mu\text{m}/8\text{ h}$  (control vs. tau 5 nM:  $p=0.0520$ , control vs. tau 15 nM:  $*p=0.0411$ , tau 5 nM vs. tau 15 nM:  $p=0.7811$ ). (c) Analysis of the migration speed in  $\mu\text{m}/\text{h}$  (control vs. tau 5 nM:  $P=0.0658$ , control vs. tau 15 nM:  $*p=0.0359$ , tau 5 nM vs. tau 15 nM:  $p=0.9576$ ). Graphs are presented as mean + SD and analyzed by one-way ANOVA with post hoc Tukey's test (b, c:  $F(2,27)=4.174$ ,  $p=0.0263$ ).  $n=3$  independent cell culture experiments with 3–4 technical replicates per experiment. ROUT test ( $Q=1\%$ ) showed no outliers. No exclusion criteria were predetermined and no samples were excluded from the analysis.

While many of these senescence features have been described in the brains of AD patients and animal models of tauopathies, a role of tau in the induction of microglial senescence has not been investigated. Here, we provide evidence that tau contributes to a senescent-like phenotype in microglia. Not only does our study confirm the senescent features presented in microglia in earlier studies on tauopathies (Brelstaff et al., 2021; Bussian et al., 2018),

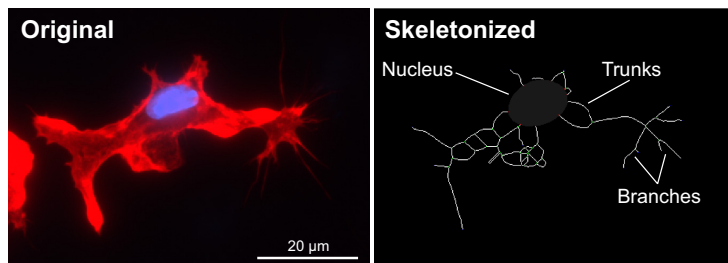
but also reveals the importance to use a combination of markers to adequately assess the occurrence of senescence. In this study, we observed an increased  $p16^{\text{INK4a}}$  and  $p21^{\text{WAF}}$  protein expression independent of the tau concentration. These findings were not reflected by the gene expression levels as we only observed changes in *Cdkn2a* ( $p16^{\text{INK4A}}$ ) after exposure to the higher tau concentration, whereas no changes were found in *Cdkn1a* ( $p21^{\text{WAF1}}$ ) expression, irrespective



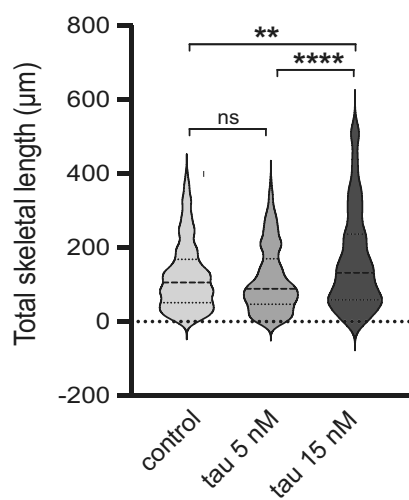
(a)



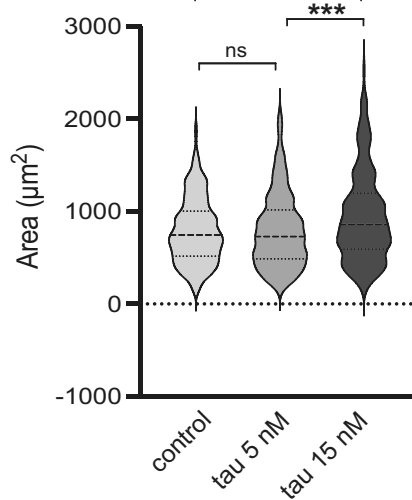
(b)



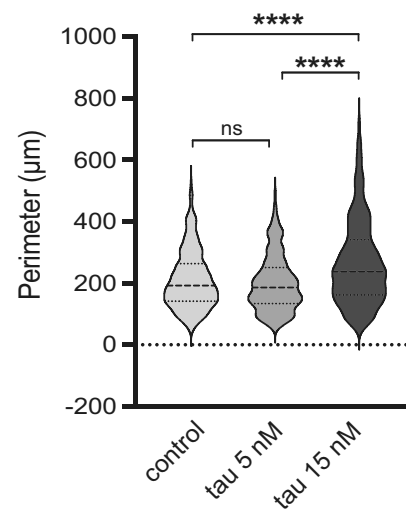
(c)



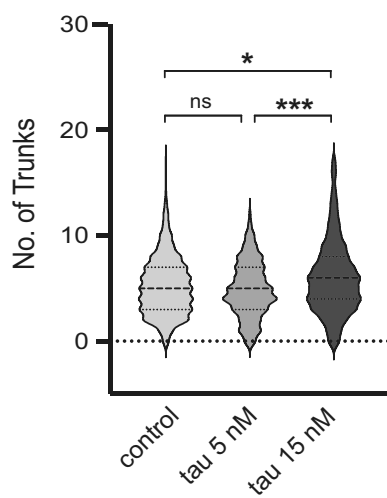
(d)



(e)



(f)



(g)

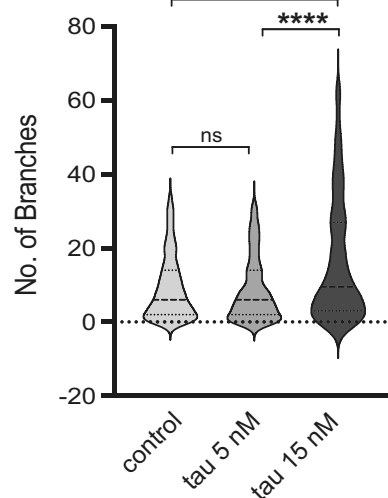


**FIGURE 6** Senescent microglia presented with a reorganization of their cytoskeleton. (a) Representative images of an immunocytochemical staining for Phalloidin (red) and DAPI (blue) in primary mouse microglia after exposure to different concentrations of tau. (b) “Original” is an example of a cell stained with Phalloidin (to label the F-actin cytoskeleton) and DAPI as nuclear counterstain. “Skeletonized” is the cell after running the skeletonization tool for morphological analysis. Dark gray is the nucleus and white are the processes that can be divided into trunks (structurally attached to the nucleus) and branches (structurally attached to trunks). (c–g) Quantification of microglial morphology, including total skeletal length (c; control vs. tau 5 nM:  $p=0.3256$ , control vs. tau 15 nM:  $^{**}p<0.0012$ , tau 5 nM vs. tau 15 nM:  $^{****}p<0.0001$ ), cell area (d; control vs. tau 5 nM:  $p>0.9999$ , control vs. tau 15 nM:  $^{***}p<0.0003$ , tau 5 nM vs. tau 15 nM:  $^{***}p<0.0002$ ), perimeter (e; control vs. tau 5 nM:  $p=0.4526$ , control vs. tau 15 nM:  $^{****}p<0.0001$ , tau 5 nM vs. tau 15 nM:  $^{****}p<0.0001$ ), number of trunks (f; control vs. tau 5 nM:  $p=0.5155$ , control vs. tau 15 nM:  $^{*}p=0.0207$ , tau 5 nM vs. tau 15 nM:  $^{***}p<0.0004$ ) and number of branches (g; control vs. tau 5 nM:  $p>0.9999$ , control vs. tau 15 nM:  $^{****}p<0.0001$ , tau 5 nM vs. tau 15 nM:  $^{****}p<0.0001$ ). Graphs are presented as violin plots and analyzed by nonparametric Kruskal–Wallis test with post hoc Dunn’s test (c: Kruskal–Wallis = 24.67,  $p<0.0001$ ; d: Kruskal–Wallis = 19.97,  $p<0.0001$ ; e: Kruskal–Wallis = 47.19,  $p<0.0001$ ; f: Kruskal–Wallis = 15.22,  $p=0.0005$ ; g: Kruskal–Wallis = 31.61,  $p<0.0001$ ). Outliers were removed (ROUT test:  $Q=1\%$ ) from all datasets. No exclusion criteria were predetermined. ns=not significant,  $n=3$  independent cell culture preparations with an estimate of 100 cells analyzed per preparation in each condition.

of the concentration used. It has been suggested that  $p21^{WAF1}$  is especially involved in the initiation while  $p16^{INK4a}$  plays a more important role in the maintenance of senescence (Stein et al., 1999), providing a potential explanation why we did not detect increased *Cdkn1a* ( $p21^{WAF1}$ ) gene expression levels in the microglia when they already acquired a senescent state. However, it seems likely that *Cdkn1a* ( $p21^{WAF1}$ ) gene expression is elevated at an earlier timepoint in our model. Furthermore, recent work revealed that individual senescent cells express a large variability in senescence-associated mRNA levels, leading to a heterogeneous senescent cell population (Cohn et al., 2022; Wiley et al., 2017). Therefore, it remains possible that a small subset of cells in our microglial population harbors increased *Cdkn1a* mRNA levels, but that this subset is too small to show changes on the population level. Nevertheless, our study addresses an important limitation to the use of gene expression analysis to identify or characterize senescent cells, thereby emphasizing the importance of using multiple biomarkers—potentially at both, mRNA and protein level—for the characterization of senescent cells.

Despite the widely accepted use of  $p16^{INK4a}$  and  $p21^{WAF1}$  to study cell cycle arrest and senescence (González-Gualda et al., 2021; Sikora et al., 2013), it is important to consider that these factors can also be upregulated upon quiescence or terminal differentiation (Blagosklonny, 2012; Ogrodnik, 2021). Both proteins have also been shown to be expressed in fibroblasts in vivo in processes related to terminal differentiation and macrophage activation (Ogrodnik, 2021). Further, ectopic expression of  $p16^{INK4a}$  was shown to induce a senescent-like state without formation of the SASP (Coppé et al., 2011). In line with those reports, our work shows that other, additional senescence-associated markers should be used. Lamin B1 is one of those markers, showing decreased protein levels in microglia only after treatment with the higher tau concentration. Given that  $p21^{WAF1}$  and lamin B1 protein levels are not in line with their respective gene expression levels raises questions about the reliability of gene expression measurements, which are often used as the main method to study senescence in tauopathies (Bussian et al., 2018; Musi et al., 2018). Interestingly, reduced lamin B1 protein levels were also found in neurons of tau-transgenic *Drosophila* (Frost et al., 2016), astrocytes of Parkinson’s Disease (PD) patients (Chinta et al., 2018) and microglia of rats bearing an amyotrophic

lateral sclerosis (ALS) linked SOD1-mutation (Trias et al., 2019). These findings, together with our work, suggest that declined levels of lamin B1 are not cell- or disease-specific, but rather a common phenomenon shared by senescent cells during neurodegenerative conditions. Moreover, we observed that microglia show increased formation of  $\gamma$ H2AX foci after treatment with the higher tau concentration.  $\gamma$ H2AX is a common marker of senescent cells, which is indicative of double-strand breaks during DNA damage (Di Micco et al., 2021; González-Gualda et al., 2021). Interestingly, increased DNA damage has been associated with the proinflammatory profile expressed by senescent cells (Ishida et al., 2019; Zhang et al., 2018). Heterochromatin remodeling is a process that has not only been observed during chronological aging but also during premature aging (Lee et al., 2020) and neurodegenerative diseases. For example, loss of H3K9me3 has been observed in neurons and astrocytes of the spinal cord and motor cortex of C9ALS/FTD BAC mice (Jury et al., 2020), a model harboring mutations present in ALS and patients. Additionally, a progressive decrease in H3K9me3 has been reported in the CA1 region of AD patients (Gil et al., 2021). Our finding that microglia treated with the higher tau concentration show reduced levels of H3K9me3 support the idea that heterochromatin loss in tauopathies could be a sign of cellular senescence in these diseases.

Cellular senescence has been shown to affect the functional abilities of the respective senescent cells. For microglia, one of their main functions is phagocytosis and clearance in response to an injury or infection or as a mechanism to shape neuronal synapses and maintain CNS homeostasis (Colonna & Butovsky, 2017; Galloway et al., 2019). Furthermore, migration to the site of insult is an important feature necessary for microglia to exert their function (Kettenmann et al., 2011; Scheiblich & Bicker, 2015). Interestingly, microglia isolated from young adult 5xFAD transgenic mice, an AD mouse model, failed to clear  $\beta$ -amyloid plaques in comparison to microglia isolated from wildtype mice (Hellwig et al., 2015). Furthermore, evidence suggests that microglia become hypophagocytic after internalizing tau aggregate-containing neurons and display a senescent-like phenotype afterward (Brelstaff et al., 2021). In line with the reports on hypophagocytic microglia in these models, treatment with the highest tau concentration resulted in microglia



with reduced tau clearance capabilities. Lastly, exposure to the highest tau concentration resulted in cytoskeleton changes in microglia, which could explain the impairments in migration distance and speed that we observed in the present study. Although not statistically significant, treatment with the lower tau concentration also impaired migration time and speed. It could be speculated that these microglia have entered an inactive, quiescent phase, which might impair their ability to effectively respond to the insult, but this remains to be investigated.

For many years, studies have placed neuroinflammation at the center of brain aging, tauopathies, and other forms of dementia (Bauer et al., 1991; Kiecolt-Glaser et al., 2003; Lasry & Ben-Neriah, 2015; Rea et al., 2018). A decade ago, researchers reported that microglial activation is one of the earliest events in a mouse model of tauopathy, even before the formation of neurofibrillary tangles (Yoshiyama et al., 2007). Later, studies have shown that soluble forms of tau, rather than fibrils, promote microglial inflammation, characterized by the release of IL-6 and IL-1 $\beta$  (Ising et al., 2019; Perea et al., 2018). Prior studies on senescence during neurodegenerative conditions reported increased *Il6* and *Il1b* gene expression levels in neurons containing NFTs (Musi et al., 2018) and microglia isolated from cortices of PS19 mice (Bussien et al., 2018). In the present study, we report that exposure to tau elicits the release of SASP factors including but not limited to IL-6 and IL-1 $\beta$ . While several SASP factors seem to be common among senescent cells, the final composition of the SASP is highly dependent on the senescence-inducing stressor as well as cell type investigated (Basisty et al., 2020; Coppé et al., 2008). Our findings highlight the secretion of at least one novel SASP factor that to the best of our knowledge has not been identified in other senescent cells so far, namely IL-27. IL-27 is a cytokine belonging to the IL-6/IL-12 family that was initially regarded as proinflammatory (Pflanz et al., 2002). One of the pathways through which IL-27 exerts its effects is via the Janus kinase (JAK)—signal transducers and activators of transcription (STAT) pathway (Morita et al., 2021). Primary human monocytes primed with IL-27 demonstrate increased TNF- $\alpha$  and IL-6 and suppressed IL-10 levels via STAT1 signaling (Kalliolias & Ivashkiv, 2008), a phenotype closely resembled by our culture model as well. Although our study did not investigate the role of IL-27-induced JAK/STAT1 signaling, it was previously shown that accumulated tau impairs synaptic function and memory performance as a result of activated JAK2/STAT1 signaling (Li et al., 2019), an effect that could potentially be exacerbated further by microglia-mediated IL-27/JAK/STAT1 signaling in neurons.

Taken together, our data suggest that a dose-dependent exposure to tau monomers induces a senescent-like phenotype including secretion of the SASP in microglia, which potentially could be involved in the inflammatory responses seen in tauopathies (Ising et al., 2019; Perea et al., 2018; Yoshiyama et al., 2007). The fact that no changes in the nuclear lamina, chromatin structure, and the SASP were observed in the lower tau concentration despite increased protein levels of p16<sup>INK4a</sup> and p21<sup>WAF1</sup> raises questions about the cellular state of these cells. While we cannot rule out that longer incubation times with our low tau concentration would finally lead to a full senescent

state, our study still shows the importance of using multiple different markers to adequately assess the senescent state of cells at a given time point. In addition, further studies are warranted to investigate the exact mechanism(s) by which monomeric tau induces senescence in microglia and how this affects bystander cells.

## AUTHOR CONTRIBUTIONS

Experiments were designed by C.I., D.K., and M.T.H. C.I., D.K., and H.S. performed the experiments and collected the data with the help of A.G., F.S., and S.S. Data analysis was performed by C.I., D.K., H.S., and M.T.H. and C.I., D.K., and M.T.H. wrote the manuscript. All authors reviewed and approved the manuscript. Funding was obtained by M.T.H. and C.I.

## ACKNOWLEDGMENTS

This work was supported by the Deutsche Forschungsgemeinschaft (DFG, German Research Foundation) under Germany's Excellence Strategy—EXC 2030—390661388 and—EXC 2151—390873048. We would like to thank the Light Microscope Facility at German Center for Neurodegenerative Diseases (DZNE) in Bonn for the microscope and analysis software. Open Access funding enabled and organized by Projekt DEAL.

## CONFLICT OF INTEREST STATEMENT

M.T.H. is a former editor for the Journal of Neurochemistry. All other authors declare no potential competing interests.

## PEER REVIEW

The peer review history for this article is available at <https://www.webofscience.com/api/gateway/wos/peer-review/10.1111/jnc.15866>.

## DATA AVAILABILITY STATEMENT

All data generated and analyzed during this study are available from the corresponding author upon reasonable request.

## ORCID

Michael T. Heneka  <https://orcid.org/0000-0003-4996-1630>

Christina Ising  <https://orcid.org/0000-0002-7267-3488>

## REFERENCES

- Alessio, N., Aprile, D., Cappabianca, S., Peluso, G., Di Bernardo, G., & Galderisi, U. (2021). Different stages of quiescence, senescence, and cell stress identified by molecular algorithm based on the expression of Ki67, RPS6, and Beta-galactosidase activity. *International Journal of Molecular Sciences*, 22, 3102.
- Arendt, T., Rödel, L., Gärtner, U., & Holzer, M. (1996). Expression of the cyclin-dependent kinase inhibitor p16 in Alzheimer's disease. *Neuroreport*, 7, 3047–3049.
- Basisty, N., Kale, A., Jeon, O. H., Kuehnemann, C., Payne, T., Rao, C., Holtz, A., Shah, S., Sharma, V., Ferrucci, L., Campisi, J., & Schilling, B. (2020). A proteomic atlas of senescence-associated secretomes for aging biomarker development. *PLoS Biology*, 18, e3000599.
- Bauer, J., Strauss, S., Schreiter-Gasser, U., Ganter, U., Schlegel, P., Witt, I., Yolk, B., & Berger, M. (1991). Interleukin-6 and





- alpha-2-macroglobulin indicate an acute-phase state in Alzheimer's disease cortices. *FEBS Letters*, 285, 111–114.
- Ben-Porath, I., & Weinberg, R. A. (2005). The signals and pathways activating cellular senescence. *The International Journal of Biochemistry & Cell Biology*, 37, 961–976.
- Blagosklonny, M. V. (2011). Cell cycle arrest is not senescence. *Aging*, 3, 94–101.
- Blagosklonny, M. V. (2012). Cell cycle arrest is not yet senescence, which is not just cell cycle arrest: Terminology for TOR-driven aging. *Aging*, 4, 159–165.
- Brelstaff, J. H., Mason, M., Katsinelos, T., McEwan, W. A., Ghetti, B., Tolkovsky, A. M., & Spillantini, M. G. (2021). Microglia become hypofunctional and release metalloproteases and tau seeds when phagocytosing live neurons with P301S tau aggregates. *Science Advances*, 7, eabg4980.
- Bussian, T. J., Aziz, A., Meyer, C. F., Swenson, B. L., van Deursen, J. M., & Baker, D. J. (2018). Clearance of senescent glial cells prevents tau-dependent pathology and cognitive decline. *Nature*, 562, 578–582.
- Caldeira, C., Cunha, C., Vaz, A. R., Falcão, A. S., Barateiro, A., Seixas, E., Fernandes, A., & Brites, D. (2017). Key aging-associated alterations in primary microglia response to Beta-amyloid stimulation. *Frontiers in Aging Neuroscience*, 9, 277.
- Caldeira, C., Oliveira, A. F., Cunha, C., Vaz, A. R., Falcão, A. S., Fernandes, A., & Brites, D. (2014). Microglia change from a reactive to an age-like phenotype with the time in culture. *Frontiers in Cellular Neuroscience*, 8, 152.
- Campisi, J., & Di Fagagna, F. D. (2007). Cellular senescence: When bad things happen to good cells. *Nature Reviews. Molecular Cell Biology*, 8, 729–740.
- Chinta, S. J., Woods, G., Demaria, M., Rane, A., Zou, Y., McQuade, A., Rajagopalan, S., Limbad, C., Madden, D. T., Campisi, J., & Andersen, J. K. (2018). Cellular senescence is induced by the environmental neurotoxin Paraquat and contributes to neuropathology linked to Parkinson's disease. *Cell Reports*, 22, 930–940.
- Cohn, R. L., Gasek, N. S., Kuchel, G. A., & Xu, M. (2022). The heterogeneity of cellular senescence: Insights at the single-cell level. *Trends in Cell Biology*, 50962–8924(22), 116–117.
- Colonna, M., & Butovsky, O. (2017). Microglia function in the central nervous system during health and neurodegeneration. *Annual Review of Immunology*, 35, 441–468.
- Coppé, J.-P., Desprez, P.-Y., Krtolica, A., & Campisi, J. (2010). The senescence-associated secretory phenotype: The dark side of tumor suppression. *Annual Review of Pathology*, 5, 99–118.
- Coppé, J.-P., Patil, C. K., Rodier, F., Sun, Y., Muñoz, D. P., Goldstein, J., Nelson, P. S., Desprez, P.-Y., & Campisi, J. (2008). Senescence-associated secretory phenotypes reveal cell-nonautonomous functions of oncogenic RAS and the p53 tumor suppressor. *PLoS Biology*, 6, e301.
- Coppé, J.-P., Rodier, F., Patil, C. K., Freund, A., Desprez, P.-Y., & Campisi, J. (2011). Tumor suppressor and aging biomarker p16(INK4a) induces cellular senescence without the associated inflammatory secretory phenotype. *The Journal of Biological Chemistry*, 286, 36396–36403.
- Cuollo, L., Antonangeli, F., Santoni, A., & Soriani, A. (2020). The senescence-associated secretory phenotype (SASP) in the challenging future of cancer therapy and age-related diseases. *Biology*, 9, 485.
- Damani, M. R., Zhao, L., Fontainhas, A. M., Amaral, J., Fariss, R. N., & Wong, W. T. (2011). Age-related alterations in the dynamic behavior of microglia. *Aging Cell*, 10, 263–276.
- Di Micco, R., Krizhanovsky, V., Baker, D., & d'Adda di Fagagna, F. (2021). Cellular senescence in ageing: From mechanisms to therapeutic opportunities. *Nature Reviews Molecular Cell Biology*, 22, 75–95.
- Farmer, K. M., Ghag, G., Puangmalai, N., Montalbano, M., Bhatt, N., & Kaye, R. (2020). P53 aggregation, interactions with tau, and impaired DNA damage response in Alzheimer's disease. *Acta Neuropathologica Communications*, 8, 132.
- Freund, A., Laberge, R.-M., Demaria, M., & Campisi, J. (2012). Lamin B1 loss is a senescence-associated biomarker. *Molecular Biology of the Cell*, 23, 2066–2075.
- Frost, B., Bardai, F. H., & Feany, M. B. (2016). Lamin dysfunction mediates neurodegeneration in Tauopathies. *Current Biology*, 26, 129–136.
- Fujimaki, K., & Yao, G. (2020). Cell dormancy plasticity: Quiescence deepens into senescence through a dimmer switch. *Physiological Genomics*, 52, 558–562.
- Galloway, D. A., Phillips, A. E. M., Owen, D. R. J., & Moore, C. S. (2019). Phagocytosis in the brain: Homeostasis and disease. *Frontiers in Immunology*, 10, 790.
- Garwood, C. J., Simpson, J. E., Al, M. S., Axe, C., Wilson, S., Heath, P. R., Shaw, P. J., et al. (2014). DNA damage response and senescence in endothelial cells of human cerebral cortex and relation to Alzheimer's neuropathology progression: A population-based study in the Medical Research Council cognitive function and ageing study (MRC-CFAS) cohort. *Neuropathology and Applied Neurobiology*, 40, 802–814.
- Gil, L., Niño, S. A., Guerrero, C., & Jiménez-Capdeville, M. E. (2021). Phospho-tau and chromatin landscapes in early and late Alzheimer's disease. *International Journal of Molecular Sciences*, 22, 10283.
- Giunta, B., Fernandez, F., Nikolic, W. V., Obregon, D., Rrapo, E., Town, T., & Tan, J. (2008). Inflammaging as a prodrome to Alzheimer's disease. *Journal of Neuroinflammation*, 5, 51.
- González-Gualda, E., Baker, A. G., Fruk, L., & Muñoz-Espín, D. (2021). A guide to assessing cellular senescence in vitro and in vivo. *The FEBS Journal*, 288, 56–80.
- Greenberg, S. B., Grove, G. L., & Cristofalo, V. J. (1977). Cell size in aging monolayer cultures. *In Vitro*, 13, 297–300.
- Hayflick, L., & Moorhead, P. S. (1961). The serial cultivation of human diploid cell strains. *Experimental Cell Research*, 25, 585–621.
- Hellwig, S., Masuch, A., Nestel, S., Katzmarski, N., Meyer-Luehmann, M., & Biber, K. (2015). Forebrain microglia from wild-type but not adult 5xFAD mice prevent amyloid- $\beta$  plaque formation in organotypic hippocampal slice cultures. *Scientific Reports*, 5, 14624.
- Heneka, M. T., Carson, M. J., El Khoury, J., Landreth, G. E., Brosseron, F., Feinstein, D. L., Jacobs, A. H., et al. (2015). Neuroinflammation in Alzheimer's disease. *Lancet Neurology*, 14, 388–405.
- Heneka, M. T., Golenbock, D. T., & Latz, E. (2015). Innate immunity in Alzheimer's disease. *Nature Immunology*, 16, 229–236.
- Heneka, M. T., Kummer, M. P., Stutz, A., Delekate, A., Schwartz, S., Vieira-Saecker, A., Griep, A., Axt, D., Remus, A., Tzeng, T. C., Gelpi, E., Halle, A., Korte, M., Latz, E., & Golenbock, D. T. (2013). NLRP3 is activated in Alzheimer's disease and contributes to pathology in APP/PS1 mice. *Nature*, 493, 674–678.
- Hernandez-Segura, A., Nehme, J., & Demaria, M. (2018). Hallmarks of cellular senescence. *Trends in Cell Biology*, 28, 436–453.
- Ishida, T., Ishida, M., Tashiro, S., & Takeishi, Y. (2019). DNA damage and senescence-associated inflammation in cardiovascular disease. *Biological & Pharmaceutical Bulletin*, 42, 531–537.
- Ising, C., Venegas, C., Zhang, S., Scheiblich, H., Schmidt, S. V., Vieira-Saecker, A., Schwartz, S., Albasset, S., McManus, R. M., Tejera, D., Griep, A., Santarelli, F., Brosseron, F., Opitz, S., Stunden, J., Merten, M., Kaye, R., Golenbock, D. T., Blum, D., ... Heneka, M. T. (2019). NLRP3 inflammasome activation drives tau pathology. *Nature*, 575, 669–673.
- Jury, N., Abarzua, S., Díaz, I., Guerra, M. V., Ampuero, E., Cubillos, P., Martinez, P., Herrera-Soto, A., Arredondo, C., Rojas, F., Manterola, M., Rojas, A., Montecino, M., Varela-Nallar, L., & van Zundert, B. (2020). Widespread loss of the silencing epigenetic mark H3K9me3 in astrocytes and neurons along with hippocampal-dependent cognitive impairment in C9orf72 BAC transgenic mice. *Clinical Epigenetics*, 12, 32.
- Kalliolias, G. D., & Ivashkiv, L. B. (2008). IL-27 activates human monocytes via STAT1 and suppresses IL-10 production but the inflammatory



- functions of IL-27 are abrogated by TLRs and p38. *Journal of Immunology*, 180, 6325–6333.
- Kamentsky, L., Jones, T. R., Fraser, A., Bray, M.-A., Logan, D. J., Madden, K. L., Ljosa, V., Rueden, C., Eliceiri, K. W., & Carpenter, A. E. (2011). Improved structure, function and compatibility for CellProfiler: Modular high-throughput image analysis software. *Bioinformatics*, 27, 1179–1180.
- Kettenmann, H., Hanisch, U.-K., Noda, M., & Verkhratsky, A. (2011). Physiology of microglia. *Physiological Reviews*, 91, 461–553.
- Kiecolt-Glaser, J. K., Preacher, K. J., MacCallum, R. C., Atkinson, C., Malarkey, W. B., & Glaser, R. (2003). Chronic stress and age-related increases in the proinflammatory cytokine IL-6. *Proceedings of the National Academy of Sciences of the United States of America*, 100, 9090–9095.
- Lasry, A., & Ben-Neriah, Y. (2015). Senescence-associated inflammatory responses: Aging and cancer perspectives. *Trends in Immunology*, 36, 217–228.
- Lee, J.-H., Kim, E. W., Croteau, D. L., & Bohr, V. A. (2020). Heterochromatin: An epigenetic point of view in aging. *Experimental & Molecular Medicine*, 52, 1466–1474.
- Lee, V. M.-Y., Goedert, M., & Trojanowski, J. Q. (2001). Neurodegenerative tauopathies. *Annual Review of Neuroscience*, 24, 1121–1159.
- Li, X.-G., Hong, X.-Y., Wang, Y.-L., Zhang, S.-J., Zhang, J.-F., Li, X.-C., Liu, Y.-C., Sun, D. S., Feng, Q., Ye, J. W., Gao, Y., Ke, D., Wang, Q., Li, H. L., Ye, K., Liu, G. P., & Wang, J. Z. (2019). Tau accumulation triggers STAT1-dependent memory deficits by suppressing NMDA receptor expression. *EMBO Reports*, 20, e47202.
- Liang, C.-C., Park, A. Y., & Guan, J.-L. (2007). In vitro scratch assay: A convenient and inexpensive method for analysis of cell migration in vitro. *Nature Protocols*, 2, 329–333.
- Mah, L.-J., El-Osta, A., & Karagiannis, T. C. (2010).  $\gamma$ H2AX as a molecular marker of aging and disease. *Epigenetics*, 5, 129–136.
- McShea, A., Harris, P. L., Webster, K. R., Wahl, A. F., & Smith, M. A. (1997). Abnormal expression of the cell cycle regulators P16 and CDK4 in Alzheimer's disease. *The American Journal of Pathology*, 150, 1933–1939.
- Morita, Y., Masters, E. A., Schwarz, E. M., & Muthukrishnan, G. (2021). Interleukin-27 and its diverse effects on bacterial infections. *Frontiers in Immunology*, 12, 678515.
- Moujabber, O., Fishbein, F., Omran, N., Liang, Y., Colmegna, I., Presley, J. F., & Stochaj, U. (2019). Cellular senescence is associated with reorganization of the microtubule cytoskeleton. *Cellular and Molecular Life Sciences*, 76, 1169–1183.
- Muñoz-Espín, D., & Serrano, M. (2014). Cellular senescence: From physiology to pathology. *Nature Reviews Molecular Cell Biology*, 15, 482–496.
- Musi, N., Valentine, J. M., Sickora, K. R., Baeuerle, E., Thompson, C. S., Shen, Q., & Orr, M. E. (2018). Tau protein aggregation is associated with cellular senescence in the brain. *Aging Cell*, 17, e12840.
- Nishio, K., & Inoue, A. (2005). Senescence-associated alterations of cytoskeleton: Extraordinary production of vimentin that anchors cytoplasmic p53 in senescent human fibroblasts. *Histochemistry and Cell Biology*, 123, 263–273.
- Ogrodnik, M. (2021). Cellular aging beyond cellular senescence: Markers of senescence prior to cell cycle arrest in vitro and in vivo. *Aging Cell*, 20, e13338.
- Perea, J. R., Ávila, J., & Bolós, M. (2018). Dephosphorylated rather than hyperphosphorylated tau triggers a pro-inflammatory profile in microglia through the p38 MAPK pathway. *Experimental Neurology*, 310, 14–21.
- Perry, V. H., & Holmes, C. (2014). Microglial priming in neurodegenerative disease. *Nature Reviews Neurology*, 10, 217–224.
- Pflanz, S., Timans, J. C., Cheung, J., Rosales, R., Kanzler, H., Gilbert, J., Hibbert, L., Churakova, T., Travis, M., Vaisberg, E., Blumenschein, W. M., Mattson, J. D., Wagner, J. L., To, W., Zurawski, S., McClanahan, T. K., Gorman, D. M., Bazan, J. F., de Waal Malefyt, R., ... Kastelein, R. A. (2002). IL-27, a heterodimeric cytokine composed of EBI3 and p28 protein, induces proliferation of naive CD4<sup>+</sup> T cells. *Immunity*, 16, 779–790.
- Rea, I. M., Gibson, D. S., McGilligan, V., McNerlan, S. E., Alexander, H. D., & Ross, O. A. (2018). Age and age-related diseases: Role of inflammation triggers and cytokines. *Frontiers in Immunology*, 9, 586.
- Reed, M. J., Ferara, N. S., & Vernon, R. B. (2001). Impaired migration, integrin function, and Actin cytoskeletal organization in dermal fibroblasts from a subset of aged human donors. *Mechanisms of Ageing and Development*, 122, 1203–1220.
- Rodier, F., Coppé, J.-P., Patil, C. K., Hoeijmakers, W. A. M., Muñoz, D. P., Raza, S. R., Freund, A., Campeau, E., Davalos, A. R., & Campisi, J. (2009). Persistent DNA damage signalling triggers senescence-associated inflammatory cytokine secretion. *Nature Cell Biology*, 11, 973–979.
- Saito, N., Araya, J., Ito, S., Tsubouchi, K., Minagawa, S., Hara, H., Ito, A., Nakano, T., Hosaka, Y., Ichikawa, A., Kadota, T., Yoshida, M., Fujita, Y., Utsumi, H., Kurita, Y., Kobayashi, K., Hashimoto, M., Wakui, H., Numata, T., ... Kuwano, K. (2019). Involvement of Lamin B1 reduction in accelerated cellular senescence during chronic obstructive pulmonary disease pathogenesis. *Journal of Immunology*, 202, 1428–1440.
- Schafer, M. J., Zhang, X., Kumar, A., Atkinson, E. J., Zhu, Y., Jachim, S., Mazula, D. L., Brown, A. K., Berning, M., Aversa, Z., Kotajarvi, B., Bruce, C. J., Greason, K. L., Suri, R. M., Tracy, R. P., Cummings, S. R., White, T. A., & LeBrasseur, N. K. (2020). The senescence-associated secretome as an indicator of age and medical risk. *JCI Insight*, 5, 133668.
- Scheiblich, H., & Bicker, G. (2015). Regulation of microglial migration, phagocytosis, and neurite outgrowth by HO-1/CO signaling. *Developmental Neurobiology*, 75, 854–876.
- Scheiblich, H., Dansokho, C., Mercan, D., Schmidt, S. V., Bousset, L., Wischhof, L., Eikens, F., Odainic, A., Spitzer, J., Griep, A., Schwartz, S., Bano, D., Latz, E., Melki, R., & Heneka, M. T. (2021). Microglia jointly degrade fibrillar alpha-synuclein cargo by distribution through tunneling nanotubes. *Cell*, 184, 5089–5106.e21.
- Shang, D., Hong, Y., Xie, W., Tu, Z., & Xu, J. (2020). Interleukin-1 $\beta$  drives cellular senescence of rat astrocytes induced by Oligomerized amyloid  $\beta$  peptide and oxidative stress. *Frontiers in Neurology*, 11, 929.
- Sidler, C., Kovalchuk, O., & Kovalchuk, I. (2017). Epigenetic regulation of cellular senescence and aging. *Frontiers in Genetics*, 8, 138.
- Sikora, E., Bielak-Zmijewska, A., & Mosieniak, G. (2013). Cellular senescence in ageing, age-related disease and longevity. *Current Vascular Pharmacology*, 12, 698–706.
- Stein, G. H., Drullinger, L. F., Soulard, A., & Dulić, V. (1999). Differential roles for cyclin-dependent kinase inhibitors p21 and p16 in the mechanisms of senescence and differentiation in human fibroblasts. *Molecular and Cellular Biology*, 19, 2109–2117.
- Streit, W. J. (2006). Microglial senescence: Does the brain's immune system have an expiration date? *Trends in Neurosciences*, 29, 506–510.
- Streit, W. J., Braak, H., Xue, Q.-S., & Bechmann, I. (2009). Dystrophic (senescent) rather than activated microglial cells are associated with tau pathology and likely precede neurodegeneration in Alzheimer's disease. *Acta Neuropathologica*, 118, 475–485.
- Su, L., Dong, Y., Wang, Y., Wang, Y., Guan, B., Lu, Y., Wu, J., et al. (2021). Potential role of senescent macrophages in radiation-induced pulmonary fibrosis. *Cell Death & Disease*, 12, 1–12.
- Terzi, M. Y., Izmirli, M., & Gogebakan, B. (2016). The cell fate: senescence or quiescence. *Molecular Biology Reports*, 43, 1213–1220.
- Trias, E., Beilby, P. R., Kovacs, M., Ibarburu, S., Varela, V., Barreto-Núñez, R., Bradford, S. C., Beckman, J. S., & Barbeito, L. (2019). Emergence of microglia bearing senescence markers during paralysis progression in a rat model of inherited ALS. *Frontiers in Aging Neuroscience*, 11, 42.
- Tsurumi, A., & Li, W. (2012). Global heterochromatin loss. *Epigenetics*, 7, 680–688.
- Ungerleider, K., Beck, J., Lissa, D., Turnquist, C., Horikawa, I., Harris, B. T., & Harris, C. C. (2021). Astrocyte senescence and SASP in



- neurodegeneration: Tau joins the loop. *Cell Cycle* Georget, 20, 752–764.
- Velarde, M. C., & Menon, R. (2016). Positive and negative effects of cellular senescence during female reproductive aging and pregnancy. *The Journal of Endocrinology*, 230, R59–R76.
- Venegas, C., Kumar, S., Franklin, B. S., Dierkes, T., Brinkschulte, R., Tejera, D., Vieira-Saecker, A., Schwartz, S., Santarelli, F., Kummer, M. P., Griep, A., Gelpi, E., Beilharz, M., Riedel, D., Golenbock, D. T., Geyer, M., Walter, J., Latz, E., & Heneka, M. T. (2017). Microglia-derived ASC specks cross-seed amyloid- $\beta$  in Alzheimer's disease. *Nature*, 552, 355–361.
- Wallis, R., Milligan, D., Hughes, B., Mizen, H., López-Domínguez, J. A., Eduputa, U., Tyler, E. J., Serrano, M., & Bishop, C. L. (2022). Senescence-associated morphological profiles (SAMPs): An image-based phenotypic profiling method for evaluating the inter and intra model heterogeneity of senescence. *Aging*, 14, 4220–4246.
- Wang, E. (1985). Are cross-bridging structures involved in the bundle formation of intermediate filaments and the decrease in locomotion that accompany cell aging? *The Journal of Cell Biology*, 100, 1466–1473.
- Wiley, C. D., Flynn, J. M., Morrissey, C., Lebofsky, R., Shuga, J., Dong, X., Unger, M. A., Vijg, J., Melov, S., & Campisi, J. (2017). Analysis of individual cells identifies cell-to-cell variability following induction of cellular senescence. *Aging Cell*, 16, 1043–1050.
- Yamada, K., Cirrito, J. R., Stewart, F. R., Jiang, H., Finn, M. B., Holmes, B. B., Binder, L. I., Mandelkow, E. M., Diamond, M. I., Lee, V. M. Y., & Holtzman, D. M. (2011). In vivo microdialysis reveals age-dependent decrease of brain interstitial fluid tau levels in P301S human tau transgenic mice. *Journal of Neuroscience*, 31, 13110–13117.
- Yang, H., Wang, H., Ren, J., Chen, Q., & Chen, Z. J. (2017). cGAS is essential for cellular senescence. *Proceedings of the National Academy of Sciences of the United States of America*, 114, E4612–E4620.
- Yoshiyama, Y., Higuchi, M., Zhang, B., Huang, S.-M., Iwata, N., Saido, T. C., Maeda, J., Suhara, T., Trojanowski, J. Q., & Lee, V. M.-Y. (2007). Synapse loss and microglial activation precede tangles in a P301S Tauopathy mouse model. *Neuron*, 53, 337–351.
- Zhang, B., Fu, D., Xu, Q., Cong, X., Wu, C., Zhong, X., Ma, Y., Lv, Z., Chen, F., Han, L., Qian, M., Chin, Y. E., Lam, E. W. F., Chiao, P., & Sun, Y. (2018). The senescence-associated secretory phenotype is potentiated by feedforward regulatory mechanisms involving Zscan4 and TAK1. *Nature Communications*, 9, 1723.
- Zhang, F., Nance, E., Alnasser, Y., Kannan, R., & Kannan, S. (2016). Microglial migration and interactions with dendrimer nanoparticles are altered in the presence of neuroinflammation. *Journal of Neuroinflammation*, 13, 65.
- Zhang, X., Liu, X., Du, Z., Wei, L., Fang, H., Dong, Q., Niu, J., et al. (2021). The loss of heterochromatin is associated with multiscale three-dimensional genome reorganization and aberrant transcription during cellular senescence. *Genome Research*, 31, 1121–1135.
- Zhang, Y., Wu, K.-M., Yang, L., Dong, Q., & Yu, J.-T. (2022). Tauopathies: New perspectives and challenges. *Molecular Neurodegeneration*, 17, 28.

## SUPPORTING INFORMATION

Additional supporting information can be found online in the Supporting Information section at the end of this article.

**How to cite this article:** Karabag, D., Scheiblich, H., Griep, A., Santarelli, F., Schwartz, S., Heneka, M. T., & Ising, C. (2023). Characterizing microglial senescence: Tau as a key player. *Journal of Neurochemistry*, 166, 517–533. <https://doi.org/10.1111/jnc.15866>